HHS Public Access

Author manuscript

J Immunol. Author manuscript; available in PMC 2020 April 15.

Published in final edited form as:

J Immunol. 2019 April 15; 202(8): 2332–2347. doi:10.4049/jimmunol.1801491.

Respiratory enterovirus (like parainfluenza virus) can cause chronic lung disease if protection by airway epithelial STAT1 is lost

Yong Zhang, **Dailing Mao**, **Shamus P. Keeler**, **Xinyu Wang**, **Kangyun Wu**, **Benjamin J. Gerovac**, **Laurie L. Shornick**, **Eugene V. Agapov**, and **Michael J. Holtzman**

Pulmonary and Critical Care Medicine, Washington University School of Medicine, St. Louis, MO 63110

Abstract

Epithelial barrier cells are proposed to be critical for host defense, and airway epithelial cell capacity for IFN signal transduction is presumed to protect against respiratory viral infection. However, it has been difficult to fully test these concepts given the absence of tools to analyze IFN signaling specific to airway epithelial cells *in vivo*. To address these issues, we generated a new line of transgenic mice with *Cre*-driver genes (*Foxj1* and *Scgb1a1*) for a floxed-*Stat1* allele (designated *Foxj1-Scgb1a1-Cre-Stat1*$^{f/f}$ mice) to target the master IFN-signal regulator STAT1 in airway epithelial cells and tested these mice for control of infection due to mouse parainfluenza (Sendai) virus (SeV) and human enterovirus (EV)-D68. Indeed, both types of infections showed increases in viral titers and severity of acute illness in *Foxj1-Scgb1a1-Cre-Stat1*$^{f/f}$ mice and conventional *Stat1*$^{-/-}$ mice compared to wild-type mice. In concert, the chronic lung disease that develops after SeV infection was also increased in *Foxj1-Scgb1a1-Cre-Stat1*$^{f/f}$ and *Stat1*$^{-/-}$ mice, marked by airway and adjacent parenchymal immune cell infiltration and mucus production for at least 7 wk after infection. Unexpectedly, relatively mild EV-D68 infection also progressed to chronic lung disease in *Foxj1-Scgb1a1-Cre-Stat1*$^{f/f}$ and *Stat1*$^{-/-}$ mice but was limited (like viral replication) to airways. The results thereby provide proof-of-concept for a critical role of barrier epithelial cells in protection from acute illness and chronic disease after viral infection and suggest a specific role for airway epithelial cells given the limitation of EV-D68 replication and acute and chronic manifestations of disease primarily to airway tissue.

Introduction

Normal function of interferon signal transduction is generally accepted as a requirement for defense against viral infections in general, and respiratory viral infections in particular (1, 2). This proposal is often based on the function of the STAT1 transcription factor that is essential for each type of IFN signaling pathway. For example, STAT1-similar to IFNR-deficiencies in transgenic mouse models results in a marked increase in susceptibility to

Address correspondence and reprint requests to Dr. Michael J. Holtzman., Washington University School of Medicine, Campus Box 8052, 660 South Euclid Avenue, St. Louis, MO 63110. mjholtzman@wustl.edu.

Conflict of Interest Disclosures

The authors have no conflicts of interest.

viral infection (3–6), including respiratory viral infection (7, 8). The central role of STAT1 in anti-viral defense is further highlighted by observations that viruses often selectively target STAT1 function to subvert the immune response (9). Moreover, molecular enhancement of STAT1 function can provide increased protection against viral infection compared to the normal physiological settings of the IFN signaling system in cell and mouse models (10). In addition, susceptibility to viral infection is also markedly increased in humans with mutations that inactivate *STAT1* gene function (11–13). Together, the critical nature of STAT1 function for anti-viral host defense is well established. What is less certain is the cellular site of action for STAT1 in the setting of infection and the implications for STAT1 function beyond the time of the acute infectious illness.

In that regard, another conventional concept for the immune system is the role of barrier epithelial cells in host defense against viral infection and the special role of airway epithelial cells in defense against respiratory viral infection. Here again, some of the best evidence for this concept was gained from loss-of-function mouse models. In particular, conventional *Stat1*$^{-/-}$ mice show increased susceptibility to severe infection with mouse parainfluenza virus also known as Sendai virus (SeV), and further, *Stat1*$^{-/-}$ mice that are reconstituted with wild-type bone marrow cells indicate that STAT1-expressing stromal cells rather than immune cells protect mice against acute illness, marked by weight loss and viral replication after this type of infection (7). Given that SeV infection can be readily detected in airway epithelial cells, these experiments provided initial evidence for these cells to account for the stromal cell function of STAT1 as a control point for respiratory viral infection. However, the experimental tools for this study were not sufficient to localize protection precisely to epithelial cells versus other stromal cells or even further to the airway epithelial cell subset since bone marrow chimeras do not provide epithelial cell-specific targeting and SeV infection is not likely to be restricted to airway epithelial cells. In addition, this initial study did not assess the development of chronic lung disease that might develop after clearance of infectious virus in relation to epithelial cells or any other cell type. This issue of long-term post-viral disease is vital to understanding how acute viral infections might initiate or exacerbate chronic airway disease, including the link between viral infection and asthma, chronic obstructive pulmonary disease (COPD), and asthma-COPD overlap syndrome in humans and whether or not the connection includes host defense compromise such as deficiencies of IFN production and/or signaling function (14, 15).

To address these issues, the present experiments were initiated to define the phenotype for STAT1 deficiency specifically in barrier epithelial cells that might serve as the primary host cells during viral infection. Within this cell population in the airway epithelium, specific candidates for viral host cells include ciliated cells that can be marked with *Foxj1* gene expression and club cells with *Scgb1a1* gene expression (16, 17). Accordingly, we generated a new line of transgenic mice with airway epithelial cell *Cre*-driver genes (*Foxj1* and *Scgb1a1*) for a floxed-*Stat1* allele (designated *Foxj1-Scgb1a1-Cre-Stat1*$^{f/f}$ mice) to determine whether STAT1 function in airway epithelial cells was required for controlling respiratory infection with SeV. We also extended this mouse model to studies of a human viral pathogen in the form of enterovirus D68 (EV-D68), a member of the Picornaviridae family that (unlike other enteroviruses) shares characteristics with human rhinovirus (RV) members of this family. In concert with shared viral features, EV-D68 can also cause

respiratory infection, and this infection can result in severe illness in susceptible populations, particularly asthmatics (18–23) as well as acute flaccid myelitis in other patients, based possibly on neuronal receptor binding (24). The severity of EV-D68-driven illness might be based on viral capacity to subvert the IFN-based immune response (25, 26), raising the possibility that any further IFN-deficiency might no longer influence the infection. In addition, to our knowledge, EV-D68 infection is limited to an acute illness. Thus, EV-D68 unlike SeV (27–30) and influenza A virus (31) has not yet been linked to the development of chronic disease that persists after clearance of infectious virus, particularly long-term respiratory disease.

Here we also aimed to define the relationship of STAT1 function and any change in acute illness to the development of chronic lung disease as a model of viral induction, exacerbation, and/or progression of the chronic airway disease. As noted above, this issue is particularly relevant to the virus-linked airway disease found in humans with asthma, COPD, or asthma-COPD overlap syndrome (32, 33). Accordingly, we focused on the cardinal features of this type of disease, i.e., airway inflammation (marked by immune cell infiltration), mucus production, (marked by mucin Muc5ac expression), hyperreactivity (marked by baseline and methacholine-induced lung resistance), and fibrosis (marked by trichrome staining) as relevant endpoints that might develop as a consequence of viral infection. We were particularly interested in airway mucus production since it appears to be linked to the earliest decline in lung function (34) and later exacerbation, progression, and death in asthma (35–39) and COPD (40–42) and to viral reprogramming of airway progenitor epithelial cells (APECs) towards mucous cells (32). Our results indicate that barrier epithelial cell capacity for STAT1 function is critical to protect against acute illness and the subsequent chronic lung disease that develops after both SeV and EV-D68 infections. The findings thereby provide proof-of-concept for the key role of barrier epithelial cells in the short-term and long-term host responses to viral infection, linking severity of acute infection to the development of chronic disease. In addition, limitation of EV-D68 infection to airway epithelial cells suggests that STAT1 protects at the level of airway versus alveolar epithelial barrier cells in the case of disease confined to airways.

Materials and Methods

Mice

Wild-type C57BL/6J mice (000664) and *Stat1*$^{-/-}$ mice (012606) mice were obtained from The Jackson Laboratory. To generate mice with *Stat1-flox* gene expression (*Stat1*$^{f/f}$), C57BL/6J genomic tail DNA was used to generate a 1.6-kb genomic DNA fragment containing *Stat1* exons 10–12, a 1.6-kb fragment upstream of exon 10 containing a *loxP* sequence as the left arm, and a 2.5 kb fragment downstream of exon 12 as the right arm using PCR-based amplification with primers derived from MGI:103063 and defined in Supplemental Table I. The *Stat1* targeting vector was assembled in a pSVloxfrtneofrt plasmid containing one *loxP* site and a Frt-flanked PGK promoter-driven *neo* gene. The homologous regions of the final vector consisted of a 1.6 kb genomic fragment, one *loxP*, exon 10, 11 and 12, loxP-frt-neo-frt and 2.5 kb genomic DNA fragment containing exon 13. The vector was transfected into C57BL/6-*LacZ* embryonic stem cells (B6/BLU, ATCC

SCRC-1019), and positive cell clones were microinjected into foster C57BL/6J mice to produce chimeric mice that were bred with C57BL/6J mice for germline transmission of the *Stat1-flox* allele based on LacZ gene expression detected with X-gal staining of RBCs as described previously (43, 44). The frt-flanked *neo* gene cassette was removed by breeding to *Flp*-deleter mice (005703), and offspring were mated with wild-type C57BL/6J mice and screened for absence of the *Flp* transgene and presence of two *loxP* sites. Heterozygotes were bred to obtain homozygous $Stat1^{f/f}$ mice that were used to prepare genomic DNA that was digested with restriction enzymes, size-separated on a 0.8% agarose Tris-Acetate-EDTA (pH 8.0) gel, and transferred onto a Biodyne nylon membrane (Pall Life Sciences) for Southern blot with 820- and 500-bp P^{32}-radiolabeled fragments immediately upstream of the left arm and downstream of the right arm, respectively, to validate homologous recombinants. The $Stat1^{f/f}$ mice were bred to *CAG-Cre* mice (019099) to generate *CAG-Cre-*$Stat1^{f/f}$ mice that were used to determine STAT1 expression across mouse tissues. The *Foxj1-Cre* mice (44) (to target ciliated cells) and *Scgb1a1-Cre* mice (45) (to target primarily club cells) were crossed to $ROSA26^{mTmG}$ reporter mice (007576) to define Cre-mediated recombination efficiency. Finally, *Foxj1-Scgb1a1-Cre* mice were crossed to $Stat1^{f/f}$ mice to generate *Foxj1-Scgb1a1-Cre-*$Stat1^{f/f}$ mice for studies of viral infection. All mice were maintained on a C57BL/6J background and were co-housed in a barrier facility using cages fitted with micro-isolator lids. Animal husbandry and experimental procedures were approved by the Animal Studies Committees of Washington University School of Medicine in accordance with the guidelines from the National Institutes of Health.

Tissue staining and microscopy

For Cre-recombination experiments, lungs from *Foxj1-Cre-*$ROSA26^{mTmG}$ and *Scgb1a1-Cre-*$ROSA26^{mTmG}$ were fixed with 10% formalin, embedded in paraffin, cut into 5-μm sections, and adhered to charged slides. Sections were deparaffinized in Fisherbrand CitroSolv (Fisher), hydrated, and treated with heat-activated antigen unmasking solution (Vector Laboratories). Immunostaining was performed using primary chicken anti-GFP antibody (Abcam), mouse anti-Foxj1 mAb from S. Brody (Washington University) (46), or goat anti-Scgb1a1 Ab (sc-9772, Santa Cruz). Primary Ab was detected with secondary Ab labeled with Alexa Fluor 594 for Foxj1 and Scgb1a1 and with Alexa Fluor 488 for GFP. Co-staining for GFP and Sftpc was performed with lung tissue that was cryopreserved in OCT compound (Tissue-Tek, Sakura Fine Tek, Torrance, CA) and then cut into 6-μm-thick sections as described previously (44), and primary rabbit anti-Sftpc Ab (ab40879, Abcam) and Alexa Fluor 647-labeled Ab (Thermo Fisher Scientific). All sections were stained with DAPI and were imaged using an Olympus BX51 microscope with a charge-coupled device camera interfaced to MagniFire software from Olympus (Melville, NY) for conventional imaging or a Zeiss LSM 880 laser scanning microscope for confocal imaging. Staining was quantified in whole lung sections using a NanoZoomer S60 slide scanner (Hamamatsu) and Image J software (47).

For viral infection experiments, immunostaining was performed using primary mouse anti-Stat1 Ab (610116, BD Biosciences), chicken anti-SeV Ab (10100648, Charles River Laboratories), mouse anti-β-Tubulin IV mAb (T7941, Sigma), goat anti-Scgb1a1 Ab (sc-9772, Santa Cruz), rabbit anti-Sftpc Ab (ab40879, Abcam), rabbit anti-EV-D68 VP1 Ab

(GTX132313, GeneTex), mouse anti-MUC5AC mAb (clone 45M1, MA 5–12175, Thermo Fisher Scientific), and rabbit anti-human CLCA1 Ab (aa 33–63). Primary Abs were detected with secondary Abs labeled with Alexa Fluor 488 (Thermo Fisher Scientific) or Alexa Fluor 594-labeled Ab (Thermo Fisher Scientific) followed by DAPI staining and immunofluorescence microscopy. Sections were also stained with hematoxylin and eosin or PAS and hematoxylin. PAS^+ staining was quantified with settings specific for the purple-magenta-tone of mucins, $Muc5ac^+$ immunostaining was quantified with a setting specific for brown tone of mucins, and $Clca1^+$ and $Muc5ac^+$ immunostaining were quantified based on fluorescence signal, each using whole lung sections and the image analysis system described above.

Virus preparation and infection

SeV was obtained from ATCC (Sendai/52 Fushimi strain, ATCC VR-105) and prepared and titered by plaque-forming assay as described previously (28). EV-D68 was identified in a clinical sample of bronchoalveolar lavage fluid with PCR and gene sequencing and was then used as a template to generate four overlapping fragments that covered the entire viral genome with RT-PCR. The fragments were cloned into a shuttle vector, and plasmid clones corresponding to the established genome sequence were placed downstream of the T7 RNA polymerase promoter and hammerhead ribozyme to produce transcripts with accurate 5'-ends (48) and poly(A) tail at the 3'end of the complete EV-D68 genome. The full-length EV-D68 genome contained identical nucleotide sequence to EV-D68 detected in the clinical sample. To generate infectious virus, the full-length genome plasmid was linearized by *NsiI* restriction enzyme digestion, and the RNA was transcribed in vitro using the MEGAscript kit (Invitrogen, CA). The DNA template was eliminated by treatment of the transcription mixture with TRIzol (Invitrogen, CA) and two rounds of DNase treatment and RNeasy (QIAgen) columns. HeLa cells were transfected with the transcribed RNA (3μg) by electroporation using GenePulser Xcell (Bio-Rad, CA). Electroporated cells were placed in a P100 dish and harvested at 24 h post-electroporation. Virus was purified by centrifugation through a sucrose cushion as described previously (49) and viral stocks were quantified using PCR assay for viral RNA and plaque-forming assay for adapted virus that is cytopathic in RD cells (ATCC CCL-136) to define equivalent PFU (ePFU) values as described previously (50).

Mice were infected with SeV (5×10^5 viruses based on qPCR assay for viral RNA equivalent to 1×10^5 PFU based on plaque-forming assay for infectious virus) or EV-D68 (1.5×10^8 viruses equivalent to 0.5×10^6 ePFU). Dosing was performing intranasally using SeV or EV-D68 in 30 μl of PBS or an equivalent amount of UV-inactivated virus (as a control for viral replication) or PBS alone under ketamine/xylazine anesthesia at 6–9 wk of age for SeV or 4 wk of age for EV-D68. Mouse age for SeV was based on previous work (27–30) and for EV-D68 was aimed at using younger but still adult mice to potentially increase susceptibility to infection just as done in other recent reports (51–53). Our approach thereby enables direct comparison across publications. Moreover, lung titers of EV-D68 RNA were no different for infection at 4 wk versus 6–9 wk of age for wild-type or *Scgb1a1-Foxj1-Cre-Stat1*$^{f/f}$ mice (data not shown). Results from male and female mice were pooled since no significant differences were found between sexes as reported initially for SeV (54)

and confirmed for SeV and EV-D68 in preliminary studies (data not shown). Mouse lungs were frozen at −70 °C for homogenization in PBS with a cell disrupter (Mini-Beadbeater-96, Biospec Products) followed by viral plaque-forming assay to track PFU level normalized to gm of lung tissue (recognizing that one mouse lung weighs approximately 100 mg) (55). Viral titers for stock solutions and lung infections were monitored by PCR assay for EV-D68 and SeV using primers defined in Supplemental Table I.

RNA analysis

Total RNA was isolated from lung tissue using the RNeasy Plus Mini kit (Qiagen) and converted to cDNA using the High-Capacity cDNA Archive kit (Life Technologies) and random hexamer primers (Applied Biosystems). Levels of viral RNA were monitored using a real-time qPCR assay for EV-D68 capsid protein (*VP1*) gene or SeV nucleoprotein (*NP*) gene with forward and reverse primers and MGB probes described in Supplemental Table I. To quantify the level of viral RNA, segments of the EV-D68 genome (nt 1–2706) or SeV genome (nt 10–1715) were cloned into plasmid pCR2.1 using the TA cloning kit (ThermoFisher Scientific) and used as standards. Lung levels of mucin *Muc5ac* mRNA were determined using real-time quantitative PCR (qPCR) assay with probes described in Supplemental Table I. All target mRNA and viral RNA levels were normalized to *Gapdh* mRNA level using the TaqMan Rodent GAPDH Control Kit. All mRNA values were expressed as fold-change normalized to *Gapdh* mRNA.

Western blot analysis

Mouse tissues were homogenized in 1% Nonidet P-40, 0.05M Tris, pH 8.0, 250 mM NaCl, and 1 mM EDTA containing Halt Protease and Phosphatase Inhibitor Cocktail (Thermo Scientific). Extracted protein was subjected to western blotting with mouse anti-Stat1 Ab (BD Biosciences) and anti-Gapdh mAb (MAB374, MilliporeSigma) detected with horseradish peroxidase-conjugated horse anti-mouse IgG Ab (7076, Cell Signaling) and enhanced chemiluminescence as described previously (10).

Airway reactivity

Airway reactivity to nebulized methacholine (Sigma, St. Louis, MO) was determined by measurements of respiratory system resistance (R_{RS}) using the FinePointe Resistance and Compliance system (DSI Buxco Research Systems, Wilmington, NC) as described previously (28, 29). Mice were anesthetized, ventilated via tracheostomy, and sequentially challenged with aerosolized PBS (baseline) followed by doubling doses of methacholine ranging from 0.6125 to 20 mg/ml. Methacholine was delivered at 3-min intervals using an in-line nebulizer (Aerogen Laboratory; 2.4–4 μm particle size). Resistance values were recorded during a 3-min period following each challenge. Data were manually verified, and spurious epochs removed from analysis.

Statistical analysis

Unless stated otherwise, all data are presented as mean ± SEM and two-tailed unpaired Student's t-test was used to assess statistical significance between means. In all cases, the threshold for statistical significance was set at a P value less than 0.05. Airway reactivity for

viral infection versus UV-inactivated virus condition was assessed using two-way analysis of variance and Bonferroni post-hoc correction.

Results

Generation of epithelial cell-specific Stat1 gene knockout mice

To determine if epithelial STAT1 function controls viral infection, we generated transgenic mice that expressed a floxed *Stat1* allele (*Stat1*$^{f/f}$) using the gene targeting scheme described in Materials and Methods and depicted in Fig. 1A. Mutant allele expression in heterozygous *Stat1*$^{wt/f}$ mice was confirmed using Southern blotting for tail DNA (Fig. 1B) In addition, crossing homozygous *Stat1*$^{f/f}$ mice to *Flp-deleter* mice and then to *CAG-Cre* mice resulted in Cre-mediated recombination with loss of STAT1 protein across lung, liver, and splenic tissues similar to conventional *Stat1*$^{-/-}$ mice based on western blotting (Fig. 1C). Together, these results validated the establishment of transgenic *Stat1*$^{f/f}$ mice with *Flp* gene deletion (hereafter referred to as *Stat1*$^{f/f}$ mice) for further study of STAT1 function *in vivo*. These mice exhibited normal birth frequency, development, and longevity without any histological changes in a full-organ survey that included lung tissue.

To define conditions for epithelial cell deletion of the *Stat1* gene, we crossed *Foxj1-Cre* mice (that target ciliated cells) and *Scgb1a1-Cre* mice (that target club cells) to *ROSA26*^{mTmG} reporter mice (Fig. 1D). Lung sections from *Foxj1-Cre-ROSA26*^{mTmG} mice immunostained with anti-Foxj1 and anti-GFP Abs showed co-localization (Fig. 1E) and a high level of co-staining (94.8% of Fojx1 cells were GFP^{+}) based on image analysis (Fig. 1F). Lung sections from *Scgb1a1-Cre-ROSA26*^{mTmG} mice immunostained for Scgb1a1, Sftpc, and GFP showed significant albeit lower levels of co-localization (Fig. 1E) and a correspondingly significant but lower level of co-staining (63.4% of Scgb1a1^{+} cells and 38.6% of Sftpc^{+} cells were GFP^{+}) based on image analysis (Fig. 1F). Each of these results was consistent with our previous analysis of *Foxj1-Cre* mice and reports of Scgb1a1-Cre activity in club and alveolar type II (AT2) cells (56). Further, the results provided a basis for establishing combined *Foxj1-Scgb1a1-Cre-Stat1*$^{f/f}$ mice to define the role of barrier epithelial cells in STAT1 function for host defense against viral infection.

Epithelial STAT1 function defends against acute SeV infection

Our initial analysis of STAT1 function showed that body weight loss was significantly enhanced in *Foxj1-Scgb1a1-Cre-Stat1*$^{f/f}$ mice compared to wild-type mice after SeV infection (Fig. 2A). In addition, body weight was decreased slightly but significantly in *Stat1*$^{-/-}$ mice compared to *Foxj1-Scgb1a1-Cre-Stat1*$^{f/f}$ mice such that *Stat1*$^{-/-}$ mice were euthanized at 8 d after infection when body weight became <70% of the initial baseline value. Similarly, survival rates were significantly decreased in *Foxj1-Scgb1a1-Cre-Stat1*$^{f/f}$ mice compared to wild-type mice after SeV infection and were decreased even further in *Stat1*$^{-/-}$ mice after SeV infection (Fig. 2B). These changes were accompanied by increases in viral titers based on lung levels of SeV-*NP* RNA in *Foxj1-Scgb1a1-Cre-Stat1*$^{f/f}$ mice compared to wild-type mice, and in turn in *Stat1*$^{-/-}$ mice compared to *Foxj1-Scgb1a1-Cre-Stat1*$^{f/f}$ mice (Fig. 2C). Similar increases in viral titers were found based on infectious virus using plaque-forming assay (Fig. 2C). In concert with body weight, survival, and viral titer

data, we also observed increases in the levels of viral immunostaining (Fig. 2D) and immune cell infiltration (Fig. 2E) in *Foxj1-Scgb1a1-Cre-Stat1*$^{f/f}$ mice and *Stat1*$^{-/-}$ mice compared to wild-type mice after SeV infection. Viral and immune cell infiltration was localized primarily to airway epithelial tissue at 3 d after infection but extended to alveolar sites by 5 d after infection, consistent with replication in both airway and alveolar epithelial cells.

To address this issue, we also used SeV co-staining with epithelial cell markers to more precisely define the site of SeV replication. In that regard, immunostaining for SeV and STAT1 was markedly increased at 3 d after SeV infection and SeV immunostaining was co-localized with STAT1 as well as ciliated cell marker β-Tubulin IV, club cell marker of Scgb1a1, and AT2 cell marker Sftpc at 3 d after infection (Fig. 3A). These results were consistent with SeV replication in ciliated cell, club cell, and AT2 cells leading to induction of STAT1 expression at these cell sites. We also found that STAT1 immunostaining was lost in ciliated cells in *Foxj1-Cre-Stat1*$^{f/f}$ mice and in both club cells and AT2 cells in *Scgb1a1-Cre-Stat1*$^{f/f}$ mice at 3 d after SeV infection (Fig. 3B), consistent with the patterns of Cre recombination observed in *Foxj1-Cre-ROSA26*^{mTmG} and *Scgb1a1-Cre-ROSA26*^{mTmG} reporter mice (Fig. 1D). Moreover, the efficiencies for Cre-mediated *Stat1* gene deletion in airway and alveolar epithelial cells (63% in club cells and 39% in AT2 cells) fit with the partial increase in severity of infection in *Foxj1-Scgb1a1-Cre-Stat1*$^{f/f}$ compared to the full increase in *Stat1*$^{-/-}$ mice. Nonetheless, the results provide a system for epithelial cell-specific deletion of *Stat1* gene expression and consequent evidence that loss of STAT1 function in barrier epithelial cells leads to increased viral replication and severity of infection.

Epithelial STAT1 function protects against SeV-induced chronic lung disease

Given the capacity of SeV infection to trigger long-term lung disease (27–30), we also continued study of *Foxj1-Scgb1a1-Cre-Stat1*$^{f/f}$ and wild-type mice that survived the acute illness due to SeV infection. Here we found that the degree of chronic lung disease was significantly increased in *Foxj1-Scgb1a1-Cre-Stat1*$^{f/f}$ mice compared to wild-type mice marked by airway and adjacent parenchymal immune cell infiltration based on hematoxylin^{+} staining in hematoxylin and eosin stained lung sections (Fig. 4A) and mucus production marked by PAS^{+} staining and mucin Muc5ac^{+} immunostaining (Fig. 4B) in lung sections at 49 d after SeV infection. Quantitative image analysis of whole lung sections demonstrated that PAS^{+} and Muc5ac^{+} areas were significantly increased in *Foxj1-Scgb1a1-Cre-Stat1*$^{f/f}$ mice compared to wild-type mice (Fig. 4C, 4D, 4E). In concert with these observations, we found that increases in Muc5ac expression were closely coordinated with increases in Clca1 expression in airway mucous cells based on immunofluorescence microscopy (Fig. 5A). Quantitative image analysis of whole lung sections confirmed that Clca1^{+} and Muc5ac^{+} areas were significantly increased in *Foxj1-Scgb1a1-Cre-Stat1*$^{f/f}$ mice compared to wild-type mice (Fig. 5B, 5C). Together, these results indicated that epithelial cell STAT1 defense against acute SeV infection also translated to protection against chronic lung disease that develops after clearance of SeV infection.

STAT1 function defends against acute EV-D68 infection

We next aimed to extend our studies of epithelial cell STAT1 to defense against respiratory viruses that are pathogenic in humans, especially in relation to severe airway disease. Given the high levels of EV-D68 replication (1×10^8-fold increase in viral titer) in primary-culture human airway epithelial cells (data not shown), we selected this virus for further study in mice *in vivo*. Initial experiments showed no significant body weight loss in *Stat1*$^{-/-}$, *Foxj1-Scgb1a1-Cre-Stat1*$^{f/f}$, or wild-type mice after EV-D68 infection (data not shown). Nonetheless, we detected significant increases in viral titer monitored by the level of EV-D68-*VP1* RNA with the largest increase in lung tissue and smaller increases in tracheal, nasal, and pharyngeal tissue in wild-type mice (Fig. 6A). In addition, we detected a time-dependent increase in EV-D68-*VP1* RNA in lung tissue with significant increases in viral RNA in *Foxj1-Scgb1a1-Cre-Stat1*$^{f/f}$ mice compared to wild-type mice, and in turn in *Stat1*$^{-/-}$ mice compared to *Foxj1-Scgb1a1-Cre-Stat1*$^{f/f}$ mice at 0.5–12 d after infection (Fig. 6B). Both time- and strain-dependence of EV-D68 titers were similar to the pattern that we found for SeV titers in lung tissue (Fig. 2C). However, the level of replication for EV-D68 was less than SeV, e.g., 1×10^1-fold versus 1×10^8-fold increase in viral RNA levels in the lung at 1 h versus 1–3 d after infection in *Stat1*$^{-/-}$ mice (Fig. 2C and Fig. 6B). Viral titer for EV-D68 was 5.7×10^7 whereas SeV was 1.2×10^4 viral RNA copies at 1 h after infection. However, this initial difference is expected since the inoculum for EV-D68 was 1.5×10^8 whereas SeV was 5.0×10^5 viral RNA copies, and the 1-h values reflect the inoculum amount since there is no detectable viral RNA replication until 4–14 h after infection (57, 58). In contrast, the viral titer at later time points is lower for EV-D68 than for SeV, but this result is also expected given the lower level of replication for a non-adapted human pathogen compared to a native rodent pathogen in a mouse host.

In concert with the increase in viral levels in lung tissue, we also observed immunostaining for EV-D68 in airway epithelium at 3 d after infection in wild-type, *Stat1*$^{-/-}$, and *Foxj1-Scgb1a1-Cre-Stat1*$^{f/f}$ mice (Fig. 6C). Moreover, EV-D68 was localized selectively to airway club cells based on co-staining with Scgb1a1 and to airway ciliated cells based on co-staining with β-Tubulin IV using conventional and confocal microscopy (Fig. 6D). Similarly, hematoxylin-eosin staining of lung sections showed immune cell infiltration mainly into the airway epithelium and adjacent subepithelial tissue at 3–8 d after infection in whole lung sections (Fig. 6E) and at higher magnification of airway epithelial sections (Fig. 6E) in all three strains of mice. Similar to viral levels, immune cell infiltration of airways was increased in *Stat1*$^{-/-}$ and *Foxj1-Scgb1a1-Cre-Stat1*$^{f/f}$ mice compared to wild-type mice at 3–8 d after EV-D68 infection (Fig. 6F). Together, these results provided evidence of productive infection with EV-D68 in mice that was confined at least primarily to airway epithelial cells and was sensitive to loss of STAT1 function in lung epithelial cells, most likely the same set of host airway epithelial cells.

Epithelial STAT1 function protects against EV-D68-induced chronic lung disease

To define whether EV-D68 infection might unexpectedly trigger long-term lung disease, we studied the possibility that excess mucus production might develop as a marker of chronic lung disease after this type of viral infection. Indeed, PAS staining of lung sections showed increases in PAS$^+$ cells (consistent with the morphology of mucous cells) in the airway

epithelium generally with adjacent immune cell infiltration in *Stat1*$^{-/-}$ and *Foxj1-Scgb1a1-Cre-Stat1*$^{f/f}$ mice at 8, 21, and 49 d after EV-D68 infection (Fig. 7A). Similarly, Muc5ac immunostaining demonstrated specific increases in Muc5ac^{+} mucous cells in the airway epithelium under these same experimental conditions (Fig. 7B). Corresponding staining of whole lung sections demonstrated that histopathologic changes marked by mucus production areas were confined to airways after EV-D68 infection (Fig. 7B, 7C). Quantitative image analysis of whole lung sections further confirmed that PAS^{+} and Muc5ac^{+} areas were significantly increased in *Stat1*$^{-/-}$ and to a lesser degree in *Foxj1-Scgb1a1-Cre-Stat1*$^{f/f}$ mice compared to wild-type mice at 8–49 d after EV-D68 infection (Fig. 7C, 7D, 7E). In concert with the evidence of chronic lung disease from tissue staining, we also found significant increases in lung levels of *Muc5ac* mRNA in *Stat1*$^{-/-}$ and to a lesser degree in *Foxj1-Scgb1a1-Cre-Stat1*$^{f/f}$ mice compared to wild-type mice at 8–49 d after EV-D68 infection (Fig. 7F). In concert with these observations, we again found that increases in Muc5ac expression were linked to increases in Clca1 expression in airway mucous cells based on immunofluorescence microscopy (Fig. 8A). Quantitative image analysis of whole lung sections confirmed that Clca1^{+} and Muc5ac^{+} areas were significantly increased in *Stat1*$^{-/-}$ and to a lesser degree in *Foxj1-Scgb1a1-Cre-Stat1*$^{f/f}$ mice at 49 d after EV-D68 infection (Fig. 8B, 8C).

In addition to immune cell infiltration and excess mucus production, we also found significant increases in airway reactivity to inhaled methacholine in *Stat1*$^{-/-}$ mice at 8 and 49 d after infection with EV-D68 compared to EV-D68-UV (Fig. 9A). Similar to the pattern observed for regulation of *Muc5ac* expression, the development of airway hyper-reactivity was not detectable in wild-type mice and was also found at only the highest concentration of methacholine in *Foxj1-Scgb1a1-Cre-Stat1*$^{f/f}$ mice (Fig. 9A). We detected no significant increase in baseline respiratory system resistance (R_{RS}) at 8 or 49 d after viral infection in wild-type, *Stat1*$^{-/-}$, or *Foxj1-Scgb1a1-Cre-Stat1*$^{f/f}$ mice (data not shown), consistent with our studies of SeV and IAV infections (28, 29, 31). To further address the comparison between the post-EV-D68 mouse model with chronic lung disease in humans, we also assessed the development of fibrosis as a feature of airway disease. Here we detected a significant increase in Gomori trichrome staining for the blue-tone of collagen expression in *Stat1*$^{-/-}$ mice at 49 d after EV-D68 infection (Fig. 9B). Corresponding staining of whole lung sections demonstrated that trichrome^{+} staining was confined to airways (Fig. 9C), and quantitative image analysis of these sections confirmed that trichrome^{+} areas were significantly increased in *Stat1*$^{-/-}$ but not *Foxj1-Scgb1a1-Cre-Stat1*$^{f/f}$ or wild-type mice at 49 d after EV-D68 infection (Fig. 9D). Together, the findings show that key features of airway disease, i.e., immune cell infiltration, mucus production, hyper-reactivity, and fibrosis can be triggered in response to EV-D68 infection if protection from STAT1 function in barrier epithelial cells is lost. The localized nature of the acute infection, chronic disease, and STAT1 deficiency in the EV-D68 model further suggests that the critical function of STAT1 to protect against these outcomes is linked in particular to airway epithelial cells.

Discussion

The present study develops key evidence that STAT1 function in barrier epithelial cells, and in particular airway epithelial cells, provides a fundamental mechanism for host defense

against respiratory viral infection and in turn a critical safeguard against chronic lung disease that develops after clearance of infectious virus. These concepts derive from a series of specific findings: (1) loss of STAT1 function in barrier epithelial cells is achieved with newly developed *Foxj1-Scgb1a1-Cre-Stat1*$^{f/f}$ transgenic mice and results in increased viral titers of both mouse and human viral pathogens (SeV and EV-D68, respectively); (2) increases in viral titers caused by epithelial STAT1 deficiency is associated with more severe acute infectious illness marked by exaggerated weight loss after SeV and immune cell infiltration after SeV and EV-D68 infections; (3) loss of STAT1 control over acute infection also leads to more severe manifestations of the chronic lung disease that can develop after clearance of SeV and EV-D68 infection and is marked by immune cell infiltration and mucus production for at least as long as 7 wk after infection; (4) STAT1-deficiency limited to epithelial cells coupled with the limitation of acute infection to airway epithelial cells (ciliated and club cells) and chronic disease to airways in the case of EV-D68 infection further suggests that STAT1 protection is specific at least in part to airway epithelial cells within the lung epithelial barrier. Here we discuss the novelty and significance of these findings for the acute infection, chronic lung disease, and implications for comparable conditions in humans.

In regard to the acute infection, we expected that global loss of STAT1 function and compromise in interferon signal transduction would lead to an increase in viral replication and titer as we described previously for SeV (7). Similarly, there was a transient delay in viral clearance in *Stat*$^{-/-}$ mice after SARS-CoV infection that persisted in bone marrow chimeras with STAT1 deficiency in stromal cells (59). Thus, as expected, we observed that both SeV and EV-D68 titers were significantly increased in conventional *Stat1*$^{-/-}$ mice compared to wild-type mice. For both types of viruses, we also found an increase in viral titer in *Foxj1-Scgb1a1-Cre-Stat1*$^{f/f}$ transgenic mice. Of note, the level of compromise was less than for *Foxj1-Scgb1a1-Cre-Stat1*$^{f/f}$ transgenic mice than *Stat1*$^{-/-}$ mice, but this result can be explained by the fact that the viruses infect both Foxj1+ ciliated cells and Scgb1a1^{+} club cells and the efficiency Cre recombination for the Scgb1a1-driver is only 63% in this cell population, consistent with previous reports by others (56). Moreover, in the case of SeV infection, the virus also infects distal Sftpc^{+} AT2 cells, and the efficiency is only 39%, thereby providing for further viral replication. In contrast, EV-D68 infection is limited to airway epithelial cells based on immunostaining for viral protein that selectively co-localizes with club cell and ciliated cell proteins in the airway epithelium. Thus, a protective effect under these conditions indicates that airway epithelial cells (rather than lung epithelial barrier cells in general) must provide a key protective site. This finding establishes long-sought evidence for this concept.

In regard to chronic lung disease, we found that the increased severity of acute infection translated to more likely and severe development of chronic lung disease that persisted after clearance of infectious virus for both SeV and EV-D68. In the case of SeV infection, the signs of chronic lung disease such as mucus production are not evident until 21 d after infection and become maximal at 49 d after infection (27–30). In contrast, for EV-D68 infection, mucus production develops during the acute infection illness at 8 d after infection and persists for at least 49 d after infection. However, this apparent difference might reflect the acute destruction of epithelium after more severe infection with SeV and hence the

inability to manifest epithelial cell differentiation towards mucous cells until there is epithelial repair by 8–12 d after infection (60). Indeed, in the case of EV-D68 infection, there were no significant signs of chronic disease unless the severity of infection was enhanced through the loss of STAT1 function using *Stat1*$^{-/-}$ or *Foxj1-Scgb1a1-Cre-Stat1*$^{f/f}$ mice. Nonetheless, despite the relatively mild nature of the acute infection with EV-D68, it is striking that signs of chronic airway disease marked by excess immune cell infiltration and mucous cell metaplasia persisted for at least 7 wk after initial infection. The limitation of EV-D68 replication to airway club and ciliated cells further provides for a specific role of airway epithelial cells in host defense and protection from lung disease. Moreover, the focal nature of the disease likely reflects localized sites of viral replication in the absence of IFN-dependent control and in turn localized reprogramming of host cells that is needed for long-term virus-induced disease.

Our findings also significantly advance previous studies of SeV, EV-D68, and related respiratory viruses in mouse models. For example, our own studies of SeV provided initial evidence that STAT1 function was required to control viral replication and acute illness based on STAT1 expression in the stromal cell compartment, but did not study epithelial cell-specific approaches or the development of chronic disease (7). Similarly, our studies of SARS-coronavirus detected increases in viral titer in *Stat1*$^{-/-}$ mice but did not define any phenotype beyond 9 d after infection (59). Similarly, a previous study detected airway neutrophil infiltration and hyperreactivity at 2 d after EV-D68 infection in female, wild-type Balbc/J mice but did not study host defense or chronic disease (61). This transient effect was slightly suppressed with anti-IL-17A blocking antibody, consistent with neutrophil-linked hyperreactivity found after short-term airway injury even in response to non-infectious agents (62), but the immune basis for subsequent longer-term disease after EV-D68 infection still needs to be defined. In contrast to the case for EV-D68, there is considerable evidence for SeV and IAV infections that the immune mechanism for post-viral disease is based on a prolonged type 2 immune response (and not an IL-17 response) that proceeds from epithelial stem cell expansion to innate immune cell activation and feed-forward to airway progenitor epithelial cell (APEC) differentiation towards mucous cells (28–31, 63). Further studies will be needed to determine whether the same mechanism drives chronic disease after EV-D68 infection. Nonetheless, the present finding for induction of *Clca1* gene expression, which is highly dependent on IL-13 stimulation (29, 31, 64, 65), suggests that the type 2 immune response might also drive chronic mucus production and airway hyper-reactivity after EV-D68 similar to SeV and IAV infections (28–31). The same mechanism is also proposed to mediate short-term airway disease after human rhinovirus (RV) infections in mice (66).

In contrast, the present model for EV-D68 infection exhibits significant viral replication, e.g., at least a 1×10^{1}-fold increase from initial viral dose and $2–3\times10^{3}$-10^{4}-fold higher viral titers for 3–8 d in *Stat1*$^{-/-}$ and *Foxj1-Scgb1a1-Cre-Stat1*$^{f/f}$ mice compared to wild-type mice. The model thereby represents an advance over mouse models for infections with closely related RVs (RV-A, RV-B, and RV-C strains) that replicate poorly in mice with peak viral titer that is generally 1×10^{3}-fold lower than the initial inoculum and is characterized by viral clearance at 4 d after infection (67–70). These results highlight the frontline role of anti-viral host defense at the airway epithelial cell barrier in controlling infection, but this system is complemented by the actions of immune cells and in particular the adaptive

immune response that allows for eventual clearance of the virus via cytotoxic T cell and antibody-producing B cell and T cell function. Presumably, at least some aspects of this adaptive immune response do not depend on IFN signal transduction and are therefore sufficient to clear infection even when initial defenses are compromised. Nonetheless, the persistently increased viral loads found with epithelial cell compromise appear to be enough to cause chronic lung disease based on the present mouse model.

The clearance of infectious virus also raises the issue of persistent viral-RNA remnants that are likely non-infectious but might still have a role in post-viral disease. In that context, we reported (and confirm here) that viral-RNA remnants are found long after clearance of infectious virus in the case of SeV (28), and we found the same persistence more recently for influenza A virus (31). In addition, our report for IAV includes data for active viral RNA replication with detection of both positive and negative-strand viral RNA and for localization of these viral-RNA remnants to sites of chronic lung disease. In each case, viral-RNA remnants are not detectable after infection with UV-inactivated virus, thereby further excluding any artifact of the PCR-based detection assay Moreover, many other labs have reported similar persistence for other RNA viruses, including RSV (73), measles virus (74), Ebola virus (75), and chikungunya virus (76). The role of active viral-RNA remnants in chronic disease is a subject of intense investigation in our lab and others. Notably, we do not detect persistence of EV-D68 RNA despite the development of chronic lung disease, suggesting that viral-RNA remnants are a marker versus a cause of long-term disease.

The present findings have significant implications for both acute illness and chronic disease that develops after viral infection and respiratory viral infection in particular in humans. In particular, EV-D68 can cause severe acute illness in humans, particularly asthmatics. The present model might therefore provide evidence that IFN-signaling deficiency is a factor in susceptibility to this type of infection. The basis for any possible IFN deficiency in asthma is less certain, but differences based on the type of infection might be highly relevant given the varying capacity of different viruses to subvert IFN production and signaling, including EV-D68 and SeV (25, 26, 71). In that context, the results provide the intriguing possibility that EV-D68 similar to SeV and IAV might be particularly prone to cause the severity of acute infection that leads to chronic disease. This experimental relationship fits with studies of viral infection in children where the type of virus does not correlate with the development of subsequent asthma (72). Additional work must particularly address, the likely scheme for viral reprogramming of APECs towards mucous cells and the possible upstream and downstream influence of immune cells. The present findings should serve as a new experimental model for these directions based on viral infections that provide significant replication and severity of illness that are key to chronic disease in the mouse model and likely in comparable airway disease due to asthma and chronic obstructive pulmonary disease.

Together, the present study establishes a new experimental model that provides proof-of-concept for the role of barrier epithelial cells in defense against respiratory viral infection based on the capacity for STAT1-dependent IFN signal transduction. The model provides for protection against acute infectious illness as well as the fundamental features of chronic respiratory disease, i.e., airway inflammation, mucus production, hyperreactivity, and

fibrosis. Thus, the model should allow further development of precise therapeutic strategies for acute and chronic lung disease in humans, ranging from gene-based to small-molecule IFN-signal enhancers to target upstream events (10, 77, 78) to cytokine- and kinase-inhibitor strategies to target downstream events such as mucous cell metaplasia (65, 79, 80). These approaches will require definition of expression and function of epithelial cell-derived cytokines in the post-EV-D68 model as was done for SeV infection and was translated to humans with COPD (29). In fact, comparison of mechanism for post-viral lung disease after EV-D68 versus SeV and IAV and related RVs will likely prove useful for stratification of patients with viral exacerbations of chronic lung disease.

Supplementary Material

Refer to Web version on PubMed Central for supplementary material.

Acknowledgements

We thank Bradford C. Bemiss and Derek E. Byers for providing human clinical samples and Xiaohua Jin and Rose M. Tidwell for expert technical assistance.

This work was supported by grants from the National Institutes of Health (National Institute of Allergy and Infectious Diseases U19-AI070412, R01-AI111605, and R01-AI130591 and National Heart, Lung, and Blood Institute R01-HL121791 and R01-HL120153).

Abbreviations used in this article:

Clca1	chloride channel accessory 1
COPD	chronic obstructive pulmonary disease
EV	enterovirus
IAV	influenza A virus
PAS	periodic acid-Schiff
qPCR	quantitative PCR
RV	rhinovirus
MUC5AC	mucin 5AC
SeV	Sendai virus

References

1. Stark GR, and Darnell JE Jr. 2012 The JAK-STAT pathway at twenty. Immunity 36: 503–514. [PubMed: 22520844]
2. Schneider WM, Chevillotte MD, and Rice CM. 2014 Interferon-stimulated genes: a complex web of host defenses. Annu. Rev. Immunol 32: 513–545. [PubMed: 24555472]
3. Durbin JE, Hackenmiller R, Simon MC, and Levy DE. 1996 Targeted disruption of the mouse Stat1 gene results in compromised innate immunity to viral disease. Cell 84: 443–450. [PubMed: 8608598]

4. Park C, Li S, Cha E, and Schindler C. 2000 Immune response in Stat2 knockout mice. Immunity 13: 795–804. [PubMed: 11163195]
5. Shimoda K, Kato K, Aoki K, Matsuda T, Miyamoto A, Shibamori M, Yamashita M, Numata A, Takase K, Kobayashi S, Shibata S, Asano Y, Gondo H, Sekigchi K, Nakayama K, Nakayama T, Okamura T, Koamura S, Niho Y, and Nakayama K. 2000 Tyk2 plays a restricted role in IFNa signaling, although it is required for IL-12-mediated T cell function. Immunity 13: 561–571. [PubMed: 11070174]
6. Durbin JE, Fernandez-Sesma A, Lee C-K, Dharma Rao T, Frey AB, Moran TM, Vukmanovic S, Garcia-Sastre A, and Levy DE. 2000 Type I IFN modulates innate and specific antiviral immunity. J. Immunol 164: 4220–4228. [PubMed: 10754318]
7. Shornick LP, Wells AG, Zhang Y, Patel AC, Huang G, Takami K, Sosa M, Shukla NA, Agapov E, and Holtzman MJ. 2008 Airway epithelial versus immune cell Stat1 function for innate defense against respiratory viral infection. J. Immunol 180: 3319–3328. [PubMed: 18292557]
8. Lee B, Gopal R, Manni ML, McHugh KJ, Mandalapu S, Robinson KM, and Alcorn JF. 2017 STAT1 is required for suppression of Type 17 immunity during influenza and bacterial superinfection. Immunohorizons 1: 81–91. [PubMed: 29577113]
9. Look DC, Roswit WT, Frick AG, Gris-Alevy Y, Dickhaus DM, Walter MJ, and Holtzman MJ. 1998 Direct suppression of Stat1 function during adenoviral infection. Immunity 9: 871–880. [PubMed: 9881977]
10. Zhang Y, Mao D, Roswit WT, Jin X, Patel AC, Patel DA, Agapov E, Wang Z, Tidwell RM, Atkinson JJ, Huang G, McCarthy R, Yu J, Yun NE, Paessler SL, Lawson TG, Omattage NS, Brett TJ, and Holtzman MJ. 2015 PARP9-DTX3L ubiquitin ligase targets host histone H2BJ and viral 3C protease to enhance interferon signaling and control viral infection. Nat. Immunol 16: 1215–1227. [PubMed: 26479788]
11. Dupuis S, Jouanguy E, Al-Hajjar S, Fieschi C, Al-Mohsen IZ, Al-Jumaah S, Yang K, Chapgier A, Eidenschenk C, Eid P, Ghonaium AA, Tufenkeji H, Frayha H, Al-Gazlan S, Al-Rayes H, Schreiber RD, Gresser I, and Casanova J-L. 2003 Impaired response to interferon-α/β and lethal viral disease in human STAT1 deficiency. Nat. Genet 33: 388–391. [PubMed: 12590259]
12. Sancho-Shimizu V, Perez de Diego R, Jouanguy E, Zhang S-Y, and Casanova J-L. 2011 Inborn errors of anti-viral interferon immunity in humans. Curr Opin Virol 1: 487–496. [PubMed: 22347990]
13. Casanova J-L, Holland SM, and Notaragelo LD. 2012 Inborn errors of human JAKS and STATs. Immunity 36: 515–528. [PubMed: 22520845]
14. Wark PA, Johnston SL, Bucchieri F, Powell R, Puddicombe S, Laza-Stanca V, Holgate ST, and Davies DE. 2005 Asthmatic bronchial epithelial cells have a deficient innate immune response to infection with rhinovirus. J. Exp. Med 201: 937–947. [PubMed: 15781584]
15. Patel DA, Huang G, Byers DE, You Y, Kim HJ, Agapov E, Moore ML, Peebles RS, Castro M, Sumino K, Shifren A, Brody SL, and Holtzman MJ. 2014 Interferon response and respiratory virus control are preserved in bronchial epithelial cells in asthma. J. Allergy Clin. Immunol 134: 1402–1412. [PubMed: 25216987]
16. You Y, Huang T, Richer EJ, Schmidt JE, Zabner J, Borok Z, and Brody SL. 2004 The role of f-box factor foxj1 in differentiation of ciliated airway epithelial cells. Am. J. Physiol. Lung Cell. Mol. Physiol 286: L650–657. [PubMed: 12818891]
17. Singh G, and Katyal SL. 1997 Clara cells and Clara cell 10 kD protein (CC10). Am. J. Respir. Cell Mol. Biol 17: 141–143. [PubMed: 9271300]
18. Imamura T, Fuji N, Suzuki A, Tamaki R, Saito M, Aniceto R, Galang H, Sombrero L, S. L, and Oshitani. H 2011 Enterovirus 68 among children with severe respiratory infection, the Phillipines. Emerg. Infect. Dis 17: 1430–1435. [PubMed: 21801620]
19. Lu Q-B, Wo Y, Wang H-Y, Wei M-T, Zhang L, Yang H, Liu E-M, Li T-Y, Zhao Z-T, Liu W, and Cao W-C. 2014 Detection of enterovirus 68 as one of the commonest types of enterovirus in patients with acute respiratory tract infection in China. J. Med. Microbiol 63: 408–414. [PubMed: 24324030]

20. Poelman R, Scholvinck EH, Borger R, Niesters HGM, and van Leer-Buter C. 2015 The emergence of enterovirus D68 in a Dutch University Medical Center and the necessity for routinely screening for respiratory viruses. J. Clin. Virol 62: 1–5. [PubMed: 25542461]
21. Schuster JE, Miller JO, Selvarangan R, Weddle G, Thompson MT, Hassan F, Rogers SL, Oberste MS, Nix WA, and Jackson MA. 2015 Severe enterovirus 68 respiratory illness in children requiring intensive care management. J. Clin. Virol 70: 77–82. [PubMed: 26305825]
22. Oermann CM, Schuster JE, Conners GP, Newland JG, Selvarangan R, and Jackson MA. 2015 Enterovirus D68: a focused review and clinical highlights from the 2014 U.S. outbreak. Ann. Am. Thorac. Soc 12: 775–781. [PubMed: 25714788]
23. Midgley CM, Watson JT, Nix WA, Curns AT, Rogers SL, Brown BA, Conover C, Dominguez SR, Feikin DR, Gray S, Hassan F, Hoferka S, Jackson MA, Johnson D, Leshem E, Miller L, Nichols JB, Nyquist A-C, Obringer E, Patel A, Patel M, Rha B, Schneider E, Schuster JE, Selvarangan R, Seward JF, Turabelidze G, Oberste MS, Pallansch MA, and Gerber SI. 2015 Severe respiratory illness associated with a nationwide outbreak of entervirus D68 in the USA (2014): a descriptive epidemiological investigation. Lancet Respir. Med 3: 879–887. [PubMed: 26482320]
24. Wei W, Guo H, Chang J, Yu Y, Liu G, Zhang N, Willard SH, Zheng S, and Yu X-F. 2016 ICAM-5/Telencephalin is a function entry receptor for enterovirus D68. Cell Host & Microbe 20: 631–841. [PubMed: 27923705]
25. Rui Y, Su J, Wang H, Chang J, Wang S, Zheng W, Cai Y, Wei W, Gordy JT, Markham R, Kong W, Zhang W, and Yu X-F. 2017 Disruption of MDA5 mediated innate immune responses by the 3C proteins of Coxsackievirus A16, Coxsackievirus A6, and Enterovirus D68. J. Virol 91: e00546–00517. [PubMed: 28424289]
26. Xiang Z, Liu L, Lei X, Zhou Z, He B, and Wang J. 2016 3C protease of enterovirus D68 inhibits cellular defense mediated by interferon regulatory factor 7. J. Virol 90: 1613–1621. [PubMed: 26608321]
27. Walter MJ, Morton JD, Kajiwara N, Agapov E, and Holtzman MJ. 2002 Viral induction of a chronic asthma phenotype and genetic segregation from the acute response. J. Clin. Invest 110: 165–175. [PubMed: 12122108]
28. Kim EY, Battaile JT, Patel AC, You Y, Agapov E, Grayson MH, Benoit LA, Byers DE, Alevy Y, Tucker J, Swanson S, Tidwell R, Tyner JW, Morton JD, Castro M, Polineni D, Patterson GA, Schwendener RA, Allard JD, Peltz G, and Holtzman MJ. 2008 Persistent activation of an innate immune response translates respiratory viral infection into chronic lung disease. Nat. Med 14: 633–640. [PubMed: 18488036]
29. Byers DE, Alexander-Brett J, Patel AC, Agapov E, Dang-Vu G, Jin X, Wu K, You Y, Alevy YG, Girard J-P, Stappenbeck TS, Patterson GA, Pierce RA, Brody SL, and Holtzman MJ. 2013 Long-term IL-33-producing epithelial progenitor cells in chronic obstructive lung disease. J. Clin. Invest 123: 3967–3982. [PubMed: 23945235]
30. Wu K, Byers DE, Jin X, Agapov E, Alexander-Brett J, Patel AC, Cella M, Gilfilan S, Colonna M, Kober DL, Brett TJ, and Holtzman MJ. 2015 TREM-2 promotes macrophage survival and lung disease after respiratory viral infection. J. Exp. Med 212: 681–697. [PubMed: 25897174]
31. Keeler SP, Agapov EV, Hinojosa ME, Letvin AN, Wu K, and Holtzman MJ. 2018 Influenza A virus infection causes chronic lung disease linked to sites of active viral RNA remnants. J. Immunol 201: 2354–2368. [PubMed: 30209189]
32. Holtzman MJ, Byers DE, Alexander-Brett J, and Wang X. 2014 The role of airway epithelial cells and innate immune cells in chronic respiratory disease. Nat. Rev. Immunol 14: 686–698. [PubMed: 25234144]
33. Woodruff PG, van den Berge M, Brightling C, Burchard EG, Christenon SA, Han MK, Holtzman MJ, Kraft M, Lynch DA, Martinez FD, Reddel HK, Sin DD, Washko GR, Wenzel SE, Punturieri A, Freemer M, and Wise RA. 2017 American Thoracic Society/National Heart, Lung, and Blood Institute asthma-chronic obstructive pulmonary disease overlap workshop report. Am. J. Respir. Crit. Care Med. 196: 375–381. [PubMed: 28636425]
34. Brito-Mutunayagam R, Appleton SL, Wilson DH, Ruffin RE, and Adams RJ. 2010 Global initiative for chronic obstructive lung disease stage 0 is associated with excess FEV1 decline in a representative population sample. Chest 138: 605–613. [PubMed: 20418365]

35. Aikawa T, Shimura S, Sasaki H, Ebina M, and Takishima T. 1992 Marked goblet cell hyperplasia with mucus accumulation in the airways of patients who died of severe acute asthma attack. Chest 101: 916–921. [PubMed: 1555462]
36. Groneberg DA, Eynott PR, Lim S, Oates T, Wu R, Carlstedt I, Roberts P, McCann B, Nicholson AG, Harrison BD, and Chung KF. 2002 Expression of respiratory mucins in fatal status asthmaticus and mild asthma. Histopathology 40: 367–373. [PubMed: 11943022]
37. Kuyper LM, Pare PD, Hogg JC, Lambert RK, Ionescu D, Woods R, and Bai TR. 2003 Characterization of airway plugging in fatal asthma. Am J Med 115: 6–11. [PubMed: 12867228]
38. James AL, Elliot JG, Abramson MJ, and Walters EH. 2005 Time to death, airway wall inflammation and remodelling in fatal asthma. Eur. Respir. J 26: 429–434. [PubMed: 16135723]
39. Dunican EM, Elicker BM, Gierada DS, Nagle SK, Schiebler ML, Newell JD, Raymond WW, Lachowicz-Scroggins ME, Di Maio S, Hoffman EA, Castro M, Fain SB, Jarjour NN, Israel E, Levy BD, Erzurum SC, Wenzel SE, Meyers DA, Bleecker ER, Phillips BR, Mauger DT, Gordon ED, Woodruff PG, Peters MC, and Fahy JV. 2018 Mucus plugs in patients with asthma linked to eosinophilia and airflow obstruction. J. Clin. Invest 128: 997–1009. [PubMed: 29400693]
40. Hogg JC, Chu F, Utokaparch S, Woods R, Elliott WM, Buzatu L, Cherniack RM, Rogers RM, Sciurba FC, Coxson HO, and Pare PD. 2004 The nature of small-airway obstruction in chronic obstructive pulmonary disease. N. Eng. J. Med 350: 2645–2653.
41. Hogg JC, Chu FS, Tan WC, Sin DD, Patel SA, Pare PD, Martinez FJ, Rogers RM, Make BJ, Criner GJ, Cherniack RM, Sharafkhaneh A, Luketich JD, Coxson HO, Elliott WM, and Sciurba FC. 2007 Survival after lung volume reduction in chronic obstructive pulmonary disease: insights from small airway pathology. Am J Respir Crit Care Med 176: 454–459. [PubMed: 17556723]
42. Kesimer M, Ford AA, Ceppe A, Radicioni G, Cao R, Davis CW, Doerschuk CM, Alexis NE, Anderson WH, Henderson AG, Barr RG, Bleecker ER, Christenson SA, Cooper CB, Han MK, Hansel NN, Hastie AT, Hoffman EA, Kanner RE, Martinez F, Paine R. r., Woodruff PG, O'Neal WK, and Boucher RC. 2017 Airway mucin concentration as a marker of chronic bronchitis. N Engl J Med 377: 911–922. [PubMed: 28877023]
43. Graubert TA, Hug BA, Wesselschmidt R, Hsieh CL, Ryan TM, Townes TM, and Ley TJ. 1998 Stochastic, stage-specific mechanisms account for the variegation of a human globin transgene. Nucl. Acids Res. 26: 2849–2858. [PubMed: 9611227]
44. Zhang Y, Huang G, Shornick LP, Roswit WT, Shipley JM, Brody SL, and Holtzman MJ. 2007 A transgenic FOXJ1-Cre system for gene inactivation in ciliated epithelial cells. (Rapid Communication). Am. J. Respir. Cell Mol. Biol 36: 515–519. [PubMed: 17255554]
45. Ji H, Houghton AM, Mariani TJ, Perera S, Kim CB, Padera R, Tonon G, McNamara K, Marconcini LA, Hezel A, El-Bardeesy N, Bronson RT, Sugarbaker D, Maser RS, Shapiro SD, and Wong K-K. 2006 K-ras activation generates an inflammatory response in lung tumors. Oncogene 25: 2105–2112. [PubMed: 16288213]
46. Pan J, You Y, Huang T, and Brody SL. 2007 RhoA-mediated apical actin enrichment is required for ciliogenesis and promoted by Foxj1. J. Cell Sci. 120: 1868–1876. [PubMed: 17488776]
47. Rueden CT, Schindelin J, Hiner MC, DeZonia BE, Walter AE, Arena ET, and Eliceiri KW. 2017 ImageJ2: ImageJ for the next generation of scientific image data. BMC Bioinformatics 18: 529. [PubMed: 29187165]
48. Herold J, and Andino R. 2000 Poliovirus requires a precise 5' end for efficient strand RNA synthesis. J. Virol 74: 6394–6400. [PubMed: 10864650]
49. Griggs TF, Bochkov YA, Nakagome K, Palmenberg AC, and Gern JE. 2015 Production, purification, and capsid stability of rhinovirus C types. J. Virol. Methods 217: 18–23. [PubMed: 25724434]
50. Liu Y, Sheng J, Baggen J, Meng G, Xiao C, Thibaut HJ, van Kuppeveld FJM, and Rossmann MG. 2015 Sialic acid-dependent cell entry of human enterovirus D68. Nat. Comm 6: 8865.
51. Evans WJ, Hurst BL, Peterson CJ, Van Wettere AJ, Day CW, Smee DF, and Tarbet EB. 2018 Development of a respiratory disease model for enterovirus D68 in 4-week-old mice for evaluation of antiviral therapies. Antiviral Res 162: 61–70. [PubMed: 30521834]

52. Morrey JD, Wang H, Hurst BL, Zukor K, Siddharthan V, Van Wettere AJ, Sinex DG, and Tarbet EB. 2018 Causation of acute flaccid paralysis by myelitis and myositis in enterovirus-D68 infected mice deficient in interferon ab/g receptor deficient mice. Viruses 10: 33.
53. Hurst BL, Evans WJ, Smee DF, and Van Wettere AJ. 2019 Evaluation of antiviral therapies in respiratory and neurological disease models of Enterovirus D68 infection in mice. Virol. 526: 146–154.
54. van Nunen MCJ, and van der Veen J. 1967 Experimental infection with Sendai virus in mice. Arch Gesamte Virusforsch 22: 388–397. [PubMed: 4300620]
55. Marino DJ 2011 Age-specific absolute and relative organ weight distributions for B6C3F1 mice. J. Toxicol. Environ. Health 75: 76–99.
56. Sinha M, and Lowell CA. 2017 Efficiency and specificity of gene deletion in lung epithelial doxycycline-inducible Cre mice. Am. J. Respir. Cell Mol. Biol 57: 248–257. [PubMed: 28287822]
57. Kato A, Kiyotani K, Sakai Y, Yoshida T, and Nagai Y. 1997 The paramxyovirus, Sendai virus, V protein encodes a luxury function required for viral pathogenesis. EMBO J 16: 578–587. [PubMed: 9034340]
58. Lu J, He Y-Q, Yi L-N, Zan H, Kung H-F, and He M-L. 2011 Viral kinetics of Enterovirus 71 in human rhabdomysarcoma cells. World J. Gastroenterol 17: 4135–4142. [PubMed: 22039330]
59. Page C, Goicochea L, Matthews K, Zhang Y, Klover P, Holtzman MJ, Hennighausen L, and Frieman M. 2012 Induction of alternatively activated macrophages enhances pathogenesis during severe acute respriatory syndrome coronavirus infection. J. Virol 86.
60. Look DC, Walter MJ, Williamson MR, Pang L, You Y, Sreshta JN, Johnson JE, Zander DS, and Brody SL. 2001 Effects of paramyxoviral infection on airway epithelial cell Foxj1 expression, ciliogenesis, and mucociliary function. Am. J. Pathol 159: 2055–2069. [PubMed: 11733356]
61. Rajput C, Han M, Bentley JK, Lei J, Ishikawa T, Wu Q, Hinde JL, Callear AP, Stillwell TL, Jackson WT, Martin ET, and Hershenson MB. 2018 Enterovirus D68 infection induces IL-17-dependent neutrophilic airway inflammation and hyperresponsiveness. JCI Insight 3: e121882.
62. O'Byrne PM, Walters EH, Gold BD, Aizawa H, Fabbri LM, Nadel JA, and Holtzman MJ. 1984 Neutrophil depletion inhibits airway hyperresponsiveness induced by ozone exposure. Am. Rev. Respir. Dis 130: 214–219. [PubMed: 6465675]
63. Byers DE, Wu K, Dang-Vu G, Jin X, Agapov E, Zhang X, Battaile JT, Schechtman KB, Yusen R, Pierce RA, and Holtzman MJ. 2018 Triggering receptor expressed on myeloid cells-2 (TREM-2) expression tracks with M2-like macrophage activity and disease severity in COPD. Chest 153: 77–86. [PubMed: 29017955]
64. Patel AC, Morton JD, Kim EY, Alevy Y, Swanson S, Tucker J, Huang G, Agapov E, Phillips TE, Fuentes ME, Iglesias A, Aud D, Allard JD, Dabbagh K, Peltz G, and Holtzman MJ. 2006 Genetic segregation of airway disease traits despite redundancy of chloride channel calcium-activated (CLCA) family members. Physiol. Genomics 25: 502–513. [PubMed: 16569774]
65. Alevy Y, Patel AC, Romero AG, Patel DA, Tucker J, Roswit WT, Miller CA, Heier RF, Byers DE, Brett TJ, and Holtzman MJ. 2012 IL-13–induced airway mucus production is attenuated by MAPK13 inhibition. J. Clin. Invest 122: 4555–4568. [PubMed: 23187130]
66. Han M, Rajput C, Hong JY, Lei J, Hinde JL, Wu Q, Bentley JK, and Hershenson MB. 2017 The innate cytokines IL-25, IL-33, and TSLP coooperate in the induction of type 2 innate lymphoid cell expansion and mucous metaplasia in rhinovirus-infected mice. J. Immunol 199: 1308–1317. [PubMed: 28701507]
67. Bartlett NW, Walton RP, Edwards MR, Aniscenko J, Caramori G, Zhu J, Glanville N, Choy KJ, Jourdan P, Burnet J, Tuthill TJ, Pedrick MS, Hurle MJ, Plumpton C, Sharp NA, Bussell JN, Swallow DM, Schwarze J, Guy B, Almond JW, Jeffrey PK, Lloyd CM, Papi A, Killington RA, Rowlands DJ, Blain ED, Clarke NJ, and Johnston SL. 2008 Mouse models of rhinovirus-induced disease and exacerbation of allergic airway inflammation. Nat. Med 14: 199–204. [PubMed: 18246079]
68. Newcomb DC, Sajjan US, Nagarkar DR, Wang Q, Nanua S, Zhou Y, McHenry CL, Hennrick KT, Tsai WC, Bentley JK, Lukacs NW, Johnston SL, and Hershenson MB. 2008 Human rhinovirus 1B exposure induces phophatidylinositol 3-kinase-dependent airway inflammation in mice. Am. J. Respir. Crit. Care Med. 177: 1111–1121. [PubMed: 18276942]

69. Wang Q, Miller DJ, Bowman ER, Nagarkar DR, Schneider D, Zhao Y, Linn MJ, Goldsmith AM, Bentley JK, Sajjan US, and Hershenson MB. 2011 MDA5 and TLR3 initiate pro-inflammatory signaling pathways leading to rhinovirus-induced airways inflammation and hyperresponsiveness. PLoS Pathog. 7: e1002070. [PubMed: 21637773]

70. Han M, Hong JY, Jaipalli S, Rajput C, Lei J, Hinde JL, Chen Q, Bentley JK, and Hershenson MB. 2016 IFN-g blocks development of an asthma phenotype in rhinovirus-infected baby mice by inhibiting type 2 innate lymphoid cells. Am. J. Respir. Cell Mol. Biol 56: 242–251.

71. Kato A, Kiyotani K, Kubota T, Yoshida T, Tashiro M, and Nagai Y. 2007 Importance of anti-interferon capacity of Sendai virus C protein for pathogenicity in mice. J Virol 81: 3264–3271. [PubMed: 17215288]

72. Bonnelykke K, Vissing NH, Sevelsted A, Johnston SL, and Bisgaard H. 2015 Association between respiratory infections in early life and later asthma is independent of virus type. J. Allergy Clin. Immunol 136: 81–86. [PubMed: 25910716]

73. Estripeaut D, Torres JP, Somers CS, Tagliabue C, Shokhar S, Bhoj VG, Grube SM, Wozniakowski A, Gomez AM, Ramilo O, Jafri HS, and Mejias A. 2008 Respiratory syncytial virus persistence in the lungs correlates with airway hyperreactivity in the mouse model. J. Inf. Dis 198: 1435–1443. [PubMed: 18828742]

74. Lin WW, Kouyos RD, Adams RJ, Grenfell BT, and Griffin DE. 2012 Prolonged persistence of measles virus RNA is characteristic of primary infection dynamics. American Review of Respiratory Disease 109: 14989–14994.

75. Jacobs M, Rodger A, Bell DJ, Bhagani S, Cropley I, Filipe A, Gifford RJ, Hopkins S, Hughes J, Johannessen JFI, Karageorgopoulos D, Lackenby A, Lester R, Liu R, MacConnachie A, Mahungu T, Martin D, Marshall N, Mepham S, Orton R, Palmarini M, Patel M, Perry C, Peters S, Porter D, Ritchie D, Ritchie N, Seaton R, Sreenu V, Templeton K, Warren S, Wilkie G, Zambon M, Gopal R, and Thomson E. 2016 Late Ebola virus relapse causing meningoencephalitis; a case report. Lancet 388: 498–503. [PubMed: 27209148]

76. Hawman DW, Fox J, Ashbrook A, May N, Schroeder K, Torres R, Crowe JJ, Dermody T, Diamond M, and Morrison T. 2016 Pathogenic Chikungunya virus evades B cell responses to establish persistence. Cell Rep 16: 1326–1338. [PubMed: 27452455]

77. Patel DA, Patel AC, Nolan WC, Zhang Y, and Holtzman MJ. 2012 High throughput screening for small molecule enhancers of the interferon signaling pathway to drive next-generation antiviral drug discovery. PloS ONE 7: e36594. [PubMed: 22574190]

78. Patel DA, Patel AC, Nolan WC, Huang G, Romero AG, Charlton N, Agapov E, Zhang Y, and Holtzman MJ. 2014 High-throughput screening normalized to biological response: application to antiviral drug discovery. J. Biomol. Screen 19: 119–130. [PubMed: 23860224]

79. Lawrence MG, Steinke JW, and Borish L. 2018 Cytokine-targeting biologics for allergic diseases. Ann Allergy Asthma Immunol 120: 376–381. [PubMed: 29410215]

80. Pavord ID 2018 Biologics and chronic obstructive pulmonary disease. J. Allergy Clin. Immunol 141: 1983–1991. [PubMed: 29729941]

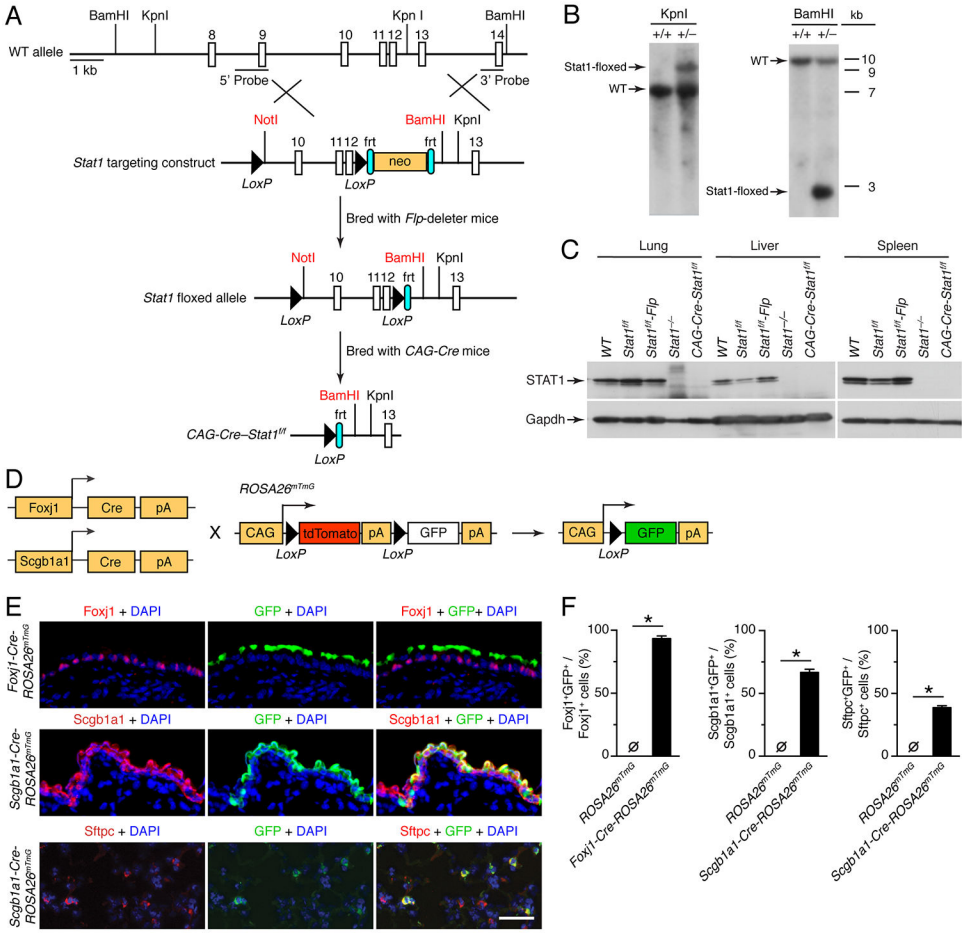

FIGURE 1.

Generation of epithelial-cell STAT1-deficient *Foxj1-Scgb1a1-Cre-Stat1*$^{f/f}$ mice. (**A**) Schematic of mouse wild-type (WT) *Stat1* gene, *Stat1* gene targeting construct, Stat1-floxed allele, and final Cre-modified *Stat1*$^{flox/flox}$ (*Cre-Stat1*$^{f/f}$) gene locus. (**B**) Southern blot of tail DNA from heterozygous *Stat1*$^{wt/f}$ and control WT mice after treatment with restriction enzymes KpnI (*Stat1*$^{f/f}$ allele size of 9 kb, WT allele size of 7 kb) or BamHI (*Stat1*$^{f/f}$ allele size of 3 kb, WT allele size of 11 kb). (**C**) Western blot of tissue homogenates from indicated mouse strains using anti-STAT1 or anti-Gapdh Ab. **(D)** Breeding scheme for *Foxj1-Cre* or *Scgb1a1-Cre* mice cross to *CAG-ROSA26*^{mTmG} mice to generate epithelial cell-specific *CAG-GFP* reporter mouse strains (*Foxj1-Cre-ROSA26*^{mTmg} and *Scgb1a1-Cre-ROSA26*^{mTmG}). (**E**) Immunostaining for Foxj1, Scgb1a1, Sfptc, and GFP and counterstain with DAPI of lung sections from *Foxj1-Cre-ROSA26*^{mTmG} or *Scgb1a1-ROSA26*^{mTmG}. Scale bar, 100 μm. **(F)** Quantitation of immunostaining for conditions in (E) along with control *ROSA26*^{mTmG} mice. For (B,C,E,F), values are representative of 3 separate experiments (n≥8 mice per condition in each experiment). For (F), * indicates $p<0.05$.

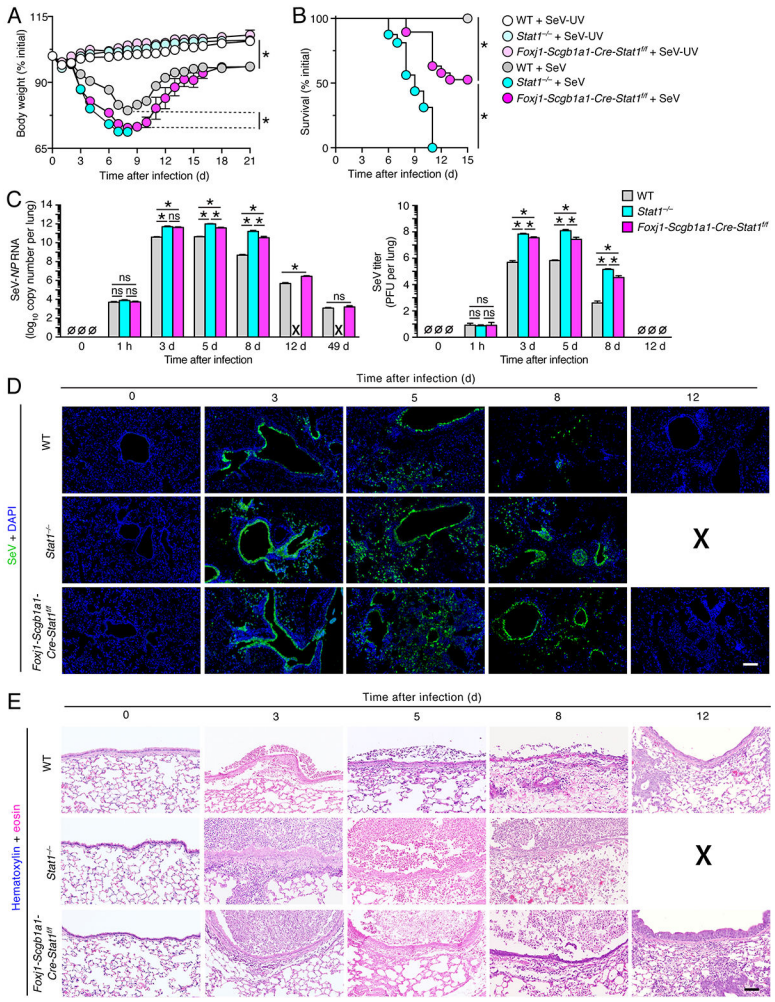

FIGURE 2.

STAT1 deficiency in epithelial cells increases severity of SeV infection. **(A)** Body weights for WT, *Stat1*$^{-/-}$, and *Foxj1-Scgb1a1-Cre-Stat1*$^{f/f}$ mice at the indicated times after infection with SeV (1×10^5 PFU given intranasally) or equivalent control SeV-UV. (**B**) Survival rates for conditions in (A). (**C**) Lung levels of SeV-*NP* RNA using PCR assay and corresponding levels of infectious SeV titers using plaque-forming assay for WT, *Stat1*$^{-/-}$, and *Foxj1-Scgb1a1-Cre-Stat1*$^{f/f}$ mice at the indicated times after infection with SeV. (**D**) Immunostaining for SeV and counterstaining with DAPI in lung sections for conditions in (C). Scale bar, 400 μm. (**E**) Hematoxylin and eosin staining in lung sections for conditions in (C). Scale bar, 200 μm. For (A-E), values are representative of 3 separate experiments (n≥8 mice per condition in each experiment). For (A-B), * indicates $p<0.05$ by ANOVA except for survival rates by Kaplan-Meier analysis, and for (C-E), X signifies data that could not be obtained due to non-survival conditions.

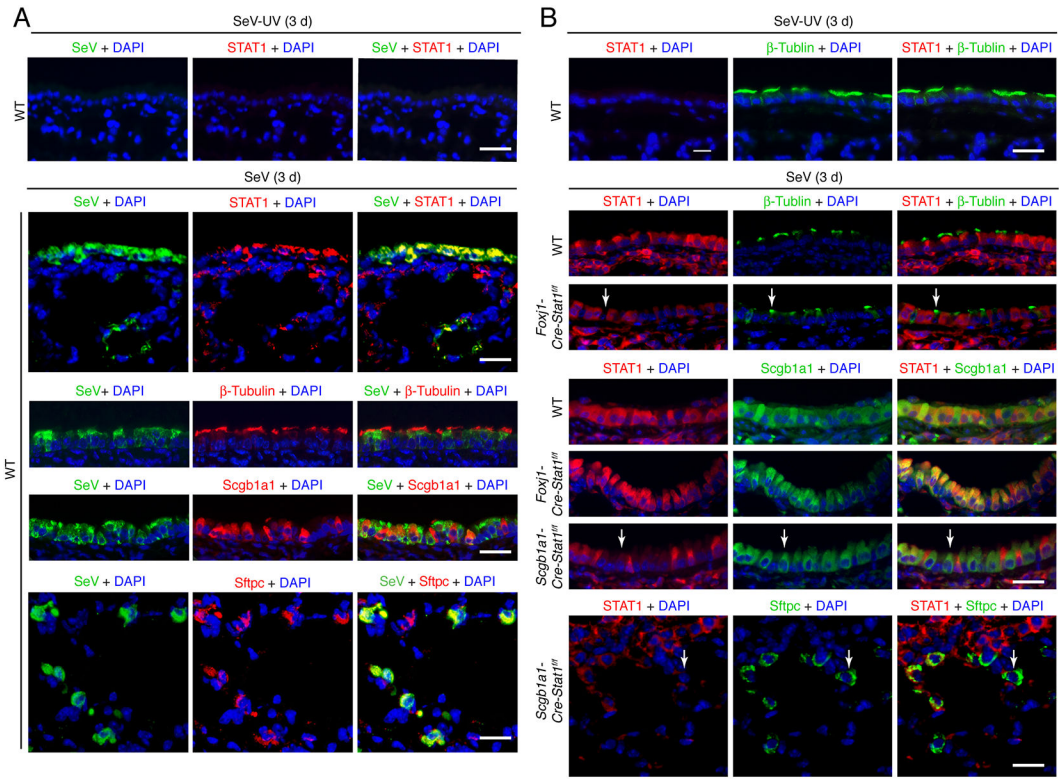

FIGURE 3.

SeV replication and STAT1 induction co-localizes to epithelial cells. (**A**) Immunostaining for SeV and STAT1, β-Tubulin IV, Scgb1a1, or Sftpc and counterstaining with DAPI in lung sections from WT mice at 3 d after infection with SeV. Scale bar, 100 μm. (**B**) Immunostaining for STAT1 and β-Tubulin IV, Scgb1a1, or Sftpc and counterstaining with DAPI in lung sections from *Foxj1-Cre-Stat1*$^{f/f}$, *Scgb1a1-Cre-Stat1*$^{f/f}$, and WT mice at 3 d after infection with SeV. Arrows indicate epithelial cells (green staining) without STAT1 (red staining) in the context of *Stat1* gene deletion. Scale bar, 100 μm. For (A,B), values are representative of 3 separate experiments (n≥8 mice per condition in each experiment).

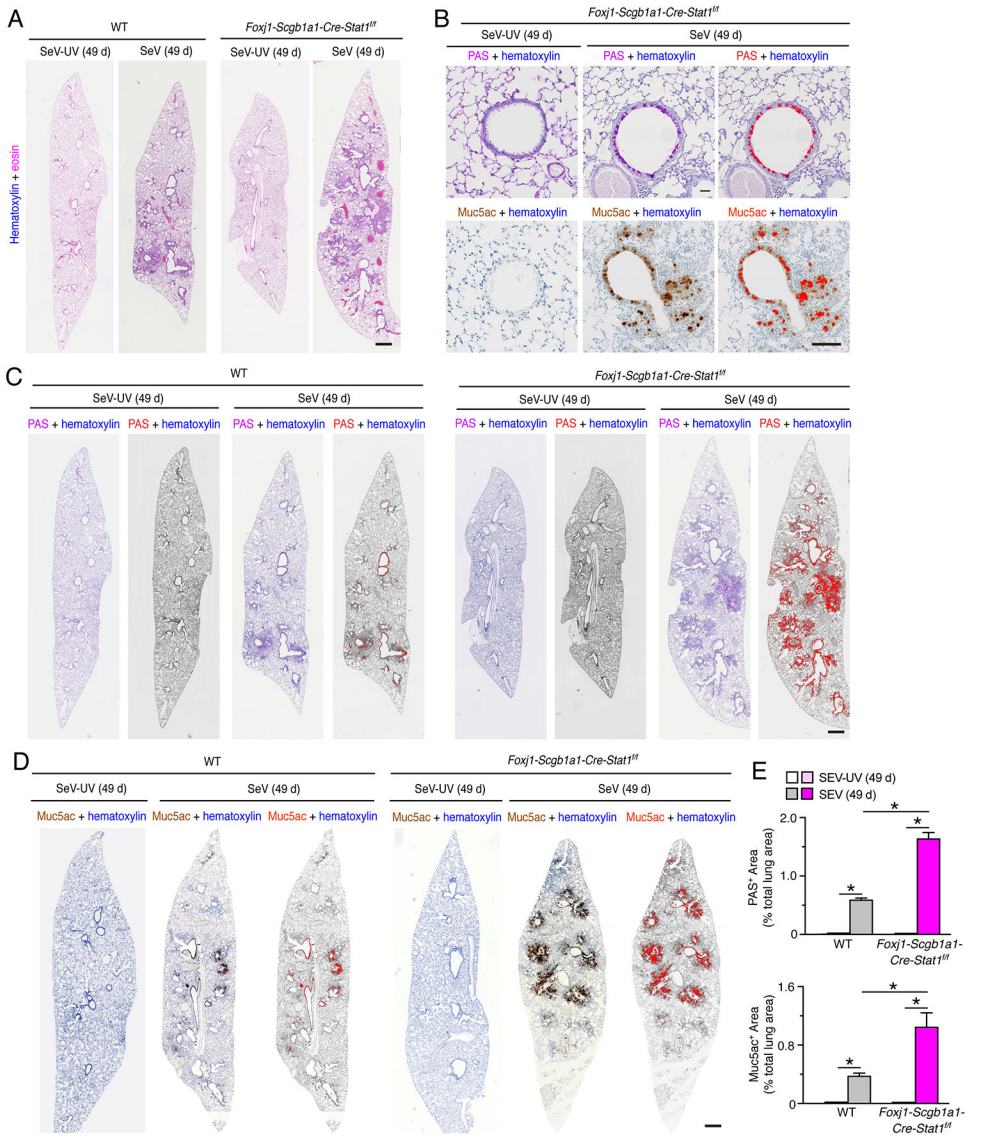

FIGURE 4.

STAT1 deficiency in epithelial cells increases susceptibility to chronic lung disease after SeV infection. (**A**) Hematoxylin and eosin staining of lung sections from WT and *Foxj1-Scgb1a1-Cre-Stat1*$^{f/f}$ mice at 49 d after infection with SeV or SeV-UV. Scale bar, 500 μm. (**B**) PAS staining and Muc5ac immunostaining for conditions in (A). Scale bar=400 μm. (**C**) PAS staining and Muc5ac immunostaining for conditions in (A). Scale bar, 500 μm. (**D**) PAS staining and Muc5ac immunostaining for conditions in (A). Scale bar, 500 μm. (**E**) Quantitation of PAS staining and Muc5ac immunostaining from conditions in (C, D). For (A-E), data are representative of 3 separate experiments (n≥8 mice per condition in each experiment). For (E), * indicates $p<0.05$.

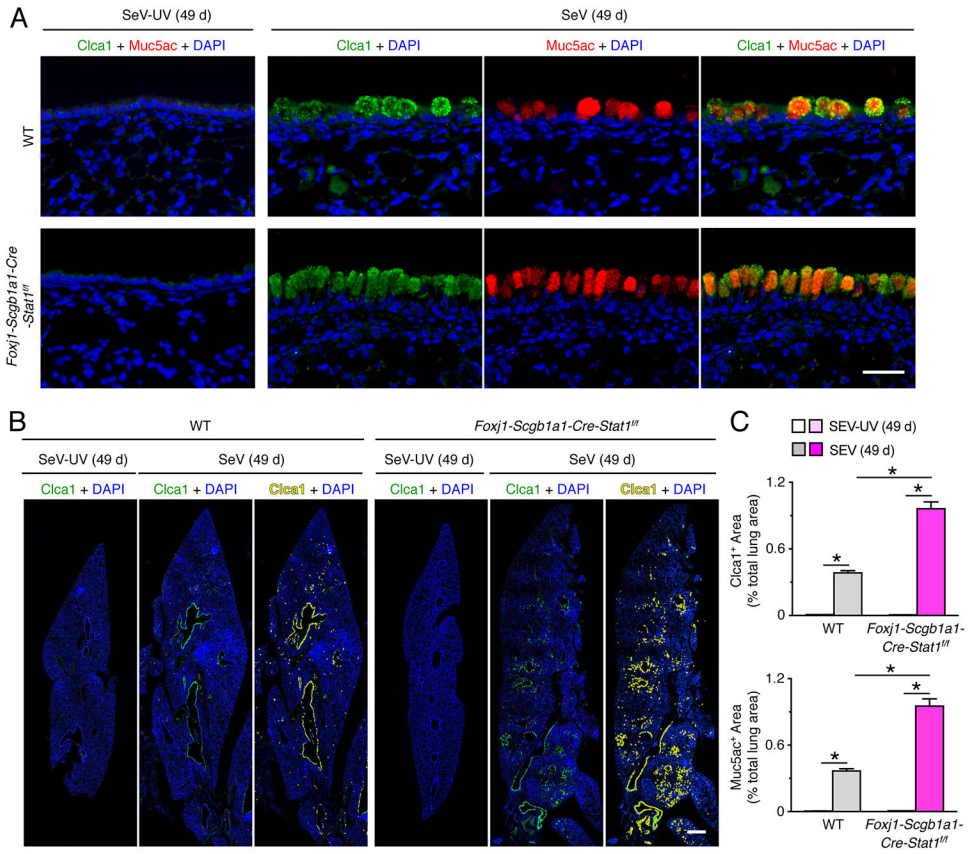

FIGURE 5.

STAT1 deficiency in epithelial cells increases susceptibility to chronic lung disease after SeV infection. (**A**)Immunostaining for Clca1 and Muc5ac and counterstaining with DAPI in lung sections from WT and *Foxj1-Scgb1a1-Cre-Stat1*$^{f/f}$ mice at 49 d after infection with SeV or SeV-UV. Scale bar, 100 μm. (**B**) Corresponding whole lung sections for Clca1 immunostaining for conditions in (A). Scale bar, 500 μm. (**C**) Quantitation of Clca1 and Muc5ac immunostaining in whole lung sections for conditions in (A). For (A-C), data are representative of 3 separate experiments (n≥8 mice per condition in each experiment). For (C), * indicates $p<0.05$.

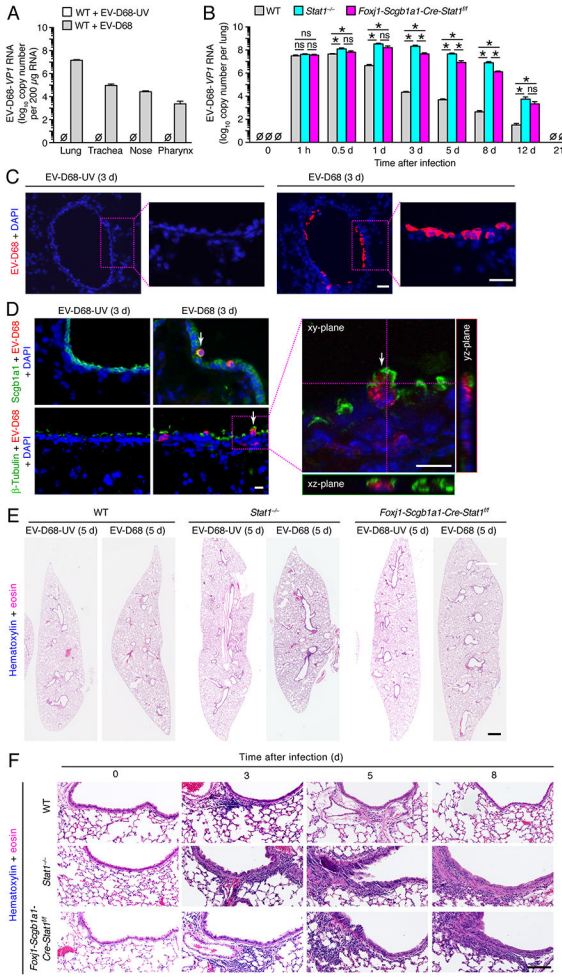

FIGURE 6.

STAT1-deficiency in epithelial cells increases severity of EV-D68 infection. (**A**) Tissue levels of EV-D68-*VP1* RNA in WT mice at 1 d after infection with EV-D68 (0.5×10^6 ePFU given intranasally) or an equivalent amount of control EV-D68-UV. (**B**) Lung levels of EV-D68-*VP1* RNA for WT, *Stat1*$^{-/-}$, and *Foxj1-Scgb1a1-Cre-Stat1*$^{f/f}$ mice at the indicated times after infection with EV-D68. (**C**) Immunostaining for EV-D68 with DAPI counterstaining in lung sections from *Stat1*$^{-/-}$ mice at 3 d after infection with EV-D68 or EV-D68-UV. Scale bar, 100 μm. (**D**) Immunostaining for EV-D68 and Scgb1a1 or β-Tubulin IV and counterstaining with DAPI in lung sections for conditions in (C) imaged with conventional and confocal microscopy. Arrows indicate cells co-staining for EV-D68 and Scgb1a1 or β-Tubulin IV. Scale bars, 50 μm. (**E**) Hematoxylin and eosin staining in lung sections for conditions in (A). Scale bar, 500 μm. (**F**) Hematoxylin and eosin staining in airway sections for conditions in (A). Scale bar, 200 μm. For (A-E), data are representative of 3 separate experiments (n≥8 mice per condition in each experiment). For (A,C), * indicates $p<0.05$.

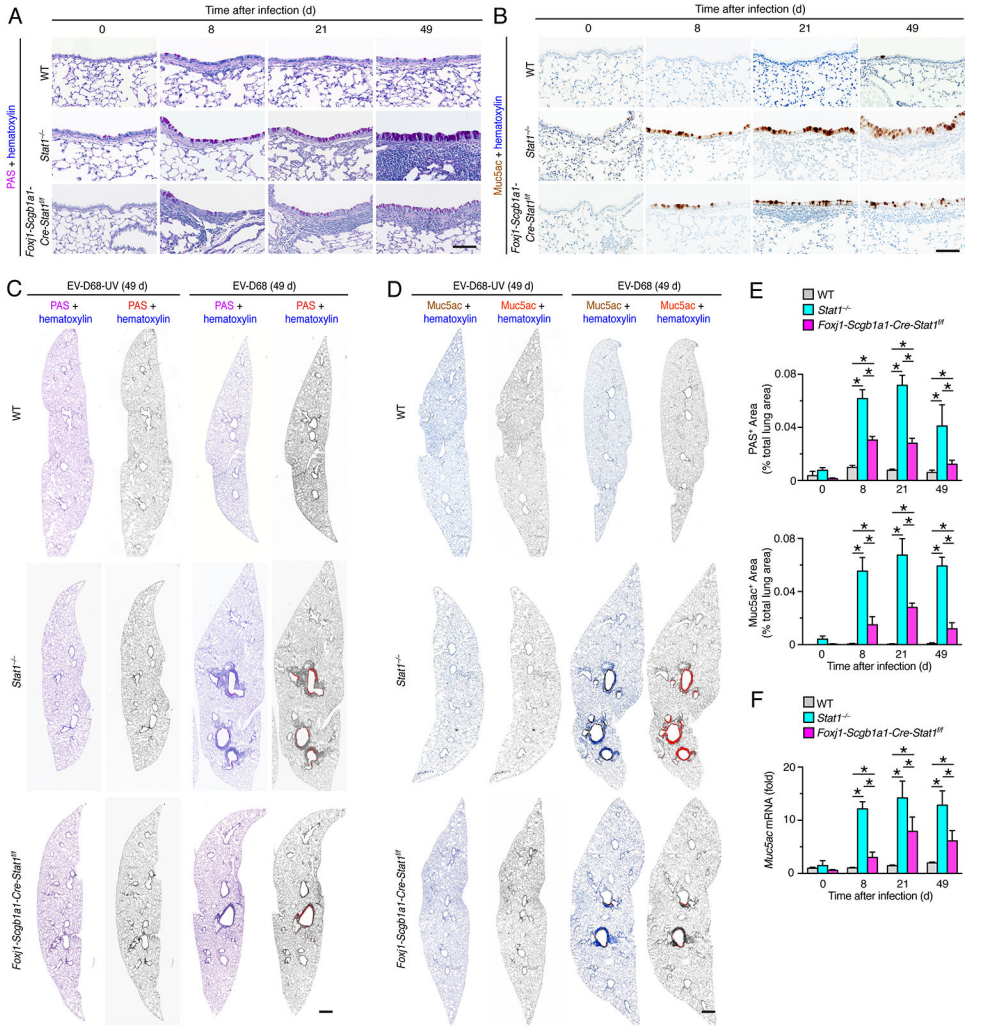

FIGURE 7.

STAT1 deficiency in epithelial cells increases susceptibility to chronic lung disease after EV-D68 infection. (**A**) PAS-hematoxylin staining of lung sections from WT, *Stat1*$^{-/-}$, and *Foxj1-Scgb1a1-Cre-Stat1*$^{f/f}$ mice at 8, 21 and 49 d after infection with EV-D68. Scale bar, 100 μm. (**B**) Muc5ac immunostaining with hematoxylin counterstaining from the conditions in (A). Scale bar, 100 μm. (**C**) PAS and hematoxylin stained lung sections from WT, *Stat1*$^{-/-}$, *Foxj1-Scgb1a1-Cre-Stat1*$^{f/f}$ mice at 49 d after infection with EV-D68 or EV-D68-UV. Scale bar, 500 μm. (**D**) Muc5ac and hematoxylin stained lung sections for conditions in (C). Scale bar, 500 μm. (**E**) Quantitation of PAS^{+} and Muc5ac^{+} staining areas for conditions in (C, D). (**F**) Lung levels of *Muc5ac* mRNA for conditions in (E). For (A-F), data are representative of 3 separate experiments (n≥8 mice per condition in each experiment). For (E,F), * indicates $p<0.05$.

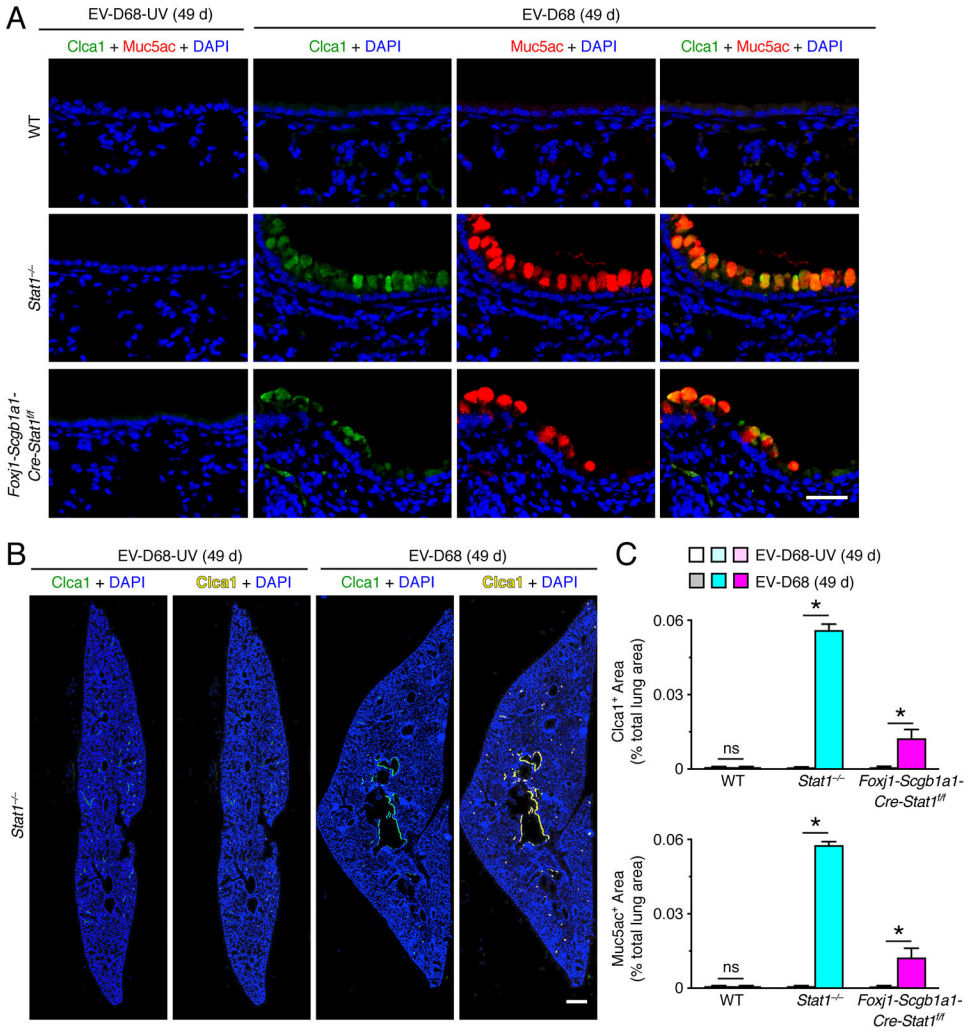

FIGURE 8.

STAT1 deficiency in epithelial cells increases susceptibility to chronic lung disease after EV-D68 infection. (**A**) Immunostaining for Clca1 and Muc5ac and counterstaining with DAPI in lung sections for WT, *Stat1*$^{-/-}$, *Foxj1-Scgb1a1-Cre-Stat1*$^{f/f}$ mice at 49 d after infection with EV-D68 or EV-D68-UV. Scale bar, 100 μm. (**B**) Corresponding whole lung sections for Clca1 immunostaining from *Stat1*$^{-/-}$ mice for conditions in (A). Scale bar, 500 μm. (**C**) Quantitation of Clca1 and Muc5ac immunostaining in whole lung sections for conditions in (A). For (A-C), data are representative of 3 separate experiments (n≥8 mice per condition in each experiment). For (C), * indicates $p<0.05$.

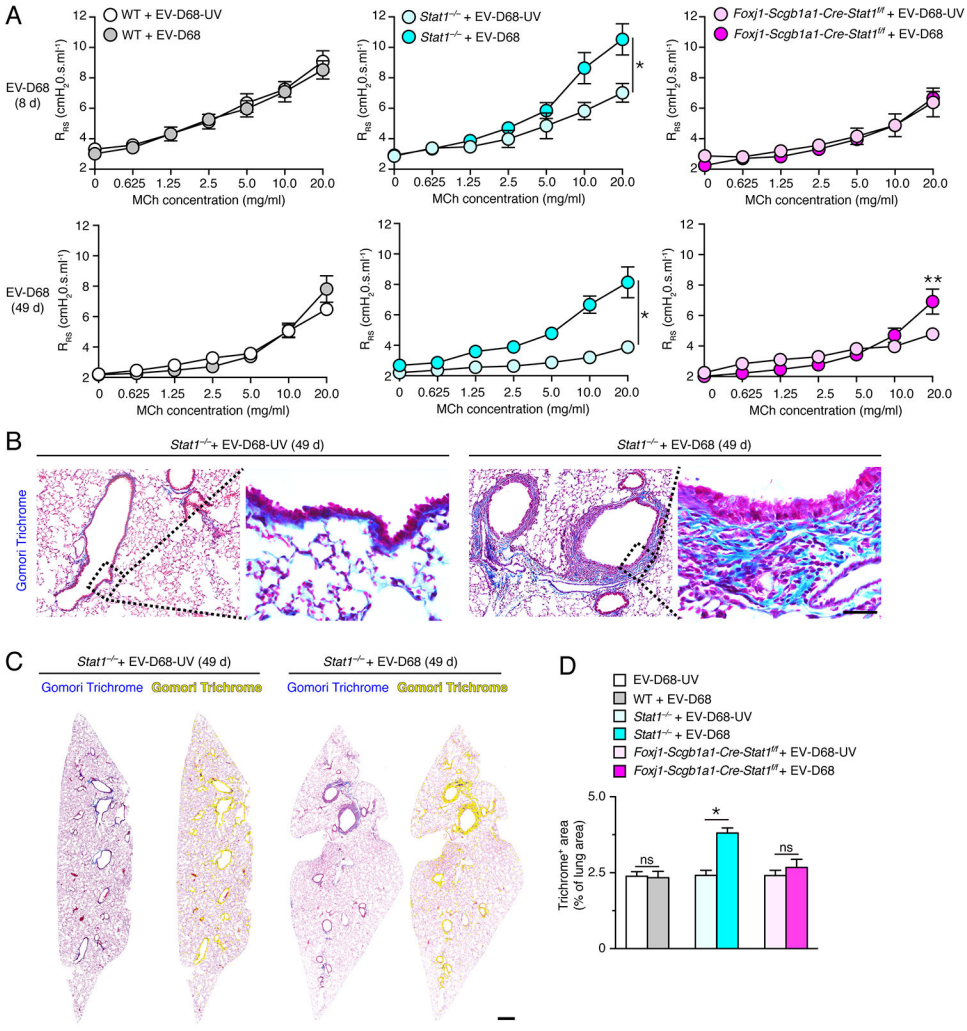

FIGURE 9.

STAT1 deficiency in epithelial cells increases susceptibility to chronic lung disease marked by airway hyperreactivity and fibrosis after EV-D68 infection. (**A**) Levels of airway reactivity using response of respiratory system resistance (R_{RS}) to inhaled methacholine (MCh) in WT, *Stat1*$^{-/-}$, and *Foxj1-Scgb1a1-Cre-Stat1*$^{f/f}$ mice at 8 d and 49 d after infection with EV-D68 or EV-D68-UV. (**B**) Gomori trichrome staining of lung sections from *Stat*$^{-/-}$ mice at 49 d after infection with EV-D68 or EV-D68-UV. Scale bar, 200 μm. (**C**) Gomori trichome staining of whole lung sections for conditions in (B) with yellow colorization indicating computer-assigned collagen-containing light-blue^{+} staining areas. Scale bar, 500 μm. (**D**) Quantitation of trichome light-blue^{+} staining areas in lung sections for WT, *Stat1*$^{-/-}$, and *Foxj1-Scgb1a1-Cre-Stat1*$^{f/f}$ mice at 49 d after infection with EV-D68 or EV-D68-UV. For (A,D), values are representative of 3 separate experiments (n=5–8 mice per condition in each experiment). For (A), * indicates $p<0.05$ by ANOVA for entire MCh concentration-response and ** indicates $p<0.05$ by post-hoc Bonferroni for single MCh concentration versus EV-D68-UV condition. For (D), * indicates $p<0.05$.